Joint Uplink and Downlink Coverage Analysis of Cellular-based RF-powered IoT Network

Mustafa A. Kishk, *Student Member, IEEE*, and Harpreet S. Dhillon, *Member, IEEE*

***Abstract*—Ambient radio frequency (RF) energy harvesting has emerged as a promising solution for powering small devices and sensors in massive Internet of Things (IoT) ecosystem due to its ubiquity and cost efficiency. In this paper, we study joint uplink and downlink coverage of cellular-based ambient RF energy harvesting IoT where the cellular network is assumed to be the only source of RF energy. We consider a time division-based approach for power and information transmission where each time-slot is partitioned into three sub-slots: 1) *charging sub-slot* during which the cellular base stations (BSs) act as RF chargers for the IoT devices, which then use the energy harvested in this sub-slot for information transmission and/or reception during the remaining two sub-slots; 2) *downlink sub-slot* during which the IoT device receives information from the associated BS; and 3) *uplink sub-slot* during which the IoT device transmits information to the associated BS. For this setup, we characterize the *joint coverage probability*, which is the joint probability of the events that the typical device harvests sufficient energy in the given time slot and is under both uplink and downlink signal-to-interference-plus-noise ratio (SINR) coverage with respect to its associated BS. This metric significantly generalizes the prior art on energy harvesting communications, which usually focused on downlink or uplink coverage separately. The key technical challenge is in handling the correlation between the amount of energy harvested in the charging sub-slot and the information signal quality (SINR) in the downlink and uplink sub-slots. Dominant BS-based approach is developed to derive tight approximation for this joint coverage probability. Several system design insights including comparison with regularly powered IoT network and throughput-optimal slot partitioning are also provided.**

***Index Terms*—Stochastic geometry, Internet of Things, ambient RF energy harvesting, cellular network, Poisson point process.**

I. Introduction

INTERNET of Things (IoT) is a massive ecosystem of interconnected *things* (referred to as IoT devices) with sensing, processing, and communication capabilities [2]. Due to its ubiquity, cellular network has emerged as an attractive option to provide reliable communication infrastructure for supporting and managing these networks [3]–[6]. This new communication paradigm will enable a new era of applications including medical applications, transportation, surveillance, and smart homes to name a few. Unlike human-operated cellular devices, such as smart phones and tablets, that can be charged at will, these IoT devices may be deployed at hard-to-reach places, such as underground or in the tunnels, which makes it difficult to charge or replace their batteries. This has led to an increasing interest in energy-efficient communication of IoT devices, both from the system design [4]–[6], and hardware perspectives [7]. While these efforts will increase the lifetime of these devices, they do not necessarily make them *self-sustained* in terms of their energy requirements. One possible way to develop an almost *self-perpetuating IoT network* is to complement or even circumvent the use of conventional batteries in the IoT devices by energy harvesting. While one can use any energy harvesting method depending upon the deployment scenario, such as solar energy, thermo-electronic, and mechanical energy [8], we focus on the ambient RF energy harvesting [9], [10], where the IoT device harvests energy through wireless RF signals. This is because of the ubiquity of RF signals even at hard-to-reach places where the other popular sources, such as solar or wind, may not be available. Besides, RF energy harvesting modules are usually cheaper to implement, which is another consideration in the deployment of IoT devices [11]. Now if RF energy harvested from the communication network (cellular network in this case) is the only source of energy, there will obviously be some new design considerations due to the limitations in the energy availability and the correlation in the communication and energy harvesting performance [12]. In this paper, we concretely expose these design considerations using tools from stochastic geometry. In particular, we define and analyze a new *joint coverage probability* metric, which significantly generalizes prior art in this area. Before going into the details of our contributions, we discuss prior art next.

A. Prior Art

Owing to their remarkable tractability and realism, tools from stochastic geometry have received significant attention over the past few years for the system-level analysis of cellular networks. Interested readers are advised to refer to [13]–[16] and the references therein for a more pedagogical treatment of this topic. More relevant subset of these works for this paper is the one that focuses on characterizing the performance of energy harvesting communication networks; see [17]–[22] for a small subset. In this subsection, we will discuss these

Manuscript received May 18, 2017; revised October 17, 2017; accepted December 12, 2017. Date of publication December 25, 2017; date of current version May 17, 2018. This work was supported by the U.S. NSF under Grant CCF-1464293. This paper was presented in part at the IEEE Globecom, Washington, DC, USA, December 2016 [1]. The associate editor coordinating the review of this paper and approving it for publication was E. Ayanoglu. *(Corresponding author: Harpreet S. Dhillon.)*

The authors are with the Wireless@VT, Department of ECE, Virginia Tech, Blacksburg, VA 24061 USA (e-mail: mkishk@vt.edu; hdhillon@vt.edu).

Digital Object Identifier 10.1109/TGCN.2017.2786694

works in the broader context of uplink, downlink, and joint uplink/downlink coverage analyses.

Uplink analysis: Most of the stochastic geometry-based works in this area are focused on the setups in which the device of interest first harvests ambient RF energy and then transmits information to its designated node (which will be its *serving BS* in the uplink cellular network) using this energy. Since the device that harvests energy is also the one that transmits information, we discuss all these works under the category of *uplink analysis* to put things in the correct context. The general theme of these works is to study the joint energy and uplink SINR coverage, which is defined as the joint probability of harvesting sufficient ambient RF energy to enable uplink transmission, and having uplink SINR above a predefined threshold. The energy and uplink SINR coverage events are independent by construction if one assumes that the ambient RF sources are placed independently of the communication network [17]–[19]. A few representative works in this direction are discussed next. Authors in [17] studied a system of energy harvesting wireless sensor network where a sensor node harvests ambient RF energy from the broadcast TV, radio, and cellular signals. The sensor node uses this energy to transmit information to a data sink located at a fixed distance. Authors in [18] studied a point-to-point (source-destination) communication link consisting of an energy harvesting source that is powered by a power beacon (PB). In particular, the source harvests power from the RF signals of PB using which it transmits information to its destination. The assumption of the existence of dedicated PBs was then generalized in [19] which studied the uplink performance of a cellular network in which mobile users are powered by a network of PBs. The other general setup, in which the prior art is significantly sparser, is the one where the same network of BSs is used for charging and communication [20], [21]. This naturally correlates the energy and uplink SINR coverage events. However, to maintain tractability, all prior works study energy and uplink coverage events separately with [20] justifying it by assuming full channel inversion power control. While such simplifications may work in specific system setups, it is desirable to handle correlation in the two coverage events properly, which will be done as a special case of our analysis.

Downlink analysis: Another general theme in the literature is to explore setups in which the device of interest first harvests ambient RF energy and then uses it to receive information. We will discuss all these works under the general category of *downlink analysis*. In small devices with severely limited power budgets, which is the case for IoT devices, energy consumption during information reception can be almost as important as the energy consumption during uplink transmission. For instance, many recent works have shown that receiver energy consumption scales noticeably with the data rates due to increase in the length of decoder interconnects [23]–[25]. Motivated by this general fact, some aspects of system design have already been explored with the consideration of receiver energy consumption, see [26]–[28] for a subset. For instance, the author in [26] used tools from stochastic geometry to study the SINR outage probability and average energy harvested under power splitting at the receiver in a system of randomly placed transmitter-receiver pairs where each transmitter has a unique receiver at a fixed distance. The main objective is to minimize the SINR outage probability subject to a constraint on the minimum average harvested energy. Authors in [27] explored power splitting receiver architecture in a point-to-point system to study the tradeoff between the average harvested energy and the average data rate. For this setup, the achievable rate-energy regions are also derived for different types of receiver architectures. Finally, [28] explored power control policies for outage minimization in a point-to-point link assuming energy harvesting at both the transmitter and the receiver. The outage is said to occur if the signal-to-noise ratio (SNR) is low or the energy harvested at the transmitter or receiver is not high enough. Contrary to all these works, which are more applicable to ad hoc or decentralized networks, the joint analysis of harvested energy and downlink SINR in a cellular setup was recently performed in [29] and [30]. In [29], since the exact analysis does not provide insightful results, authors use Frechet's inequality to derive an upper bound on the joint downlink energy and SINR coverage probability. In this paper, we will derive joint energy and downlink SINR coverage probability as the special case of our general result.

As is evident from the above discussion, all the prior works on stochastic geometry-based analyses of cellular networks with energy harvesting users/devices are either focused on uplink or downlink. To the best of our knowledge, there is no work that deals with joint uplink/downlink coverage probability defined by the joint energy, uplink SINR, and downlink SINR coverage probability, which is the main focus of this paper. That being said, the joint downlink and uplink coverage has received some attention recently in the *regularly powered networks*[1] [31]–[33]. For instance, authors in [31] use a 3GPP simulation model to determine whether it is appropriate to assume independence in the uplink and downlink coverage events. The simulation results demonstrate that the two events cannot be treated as independent. This is due to the correlation that results from associating with the same BS in both uplink and downlink. Sometimes this correlation is ignored in the interest of tractability. For instance, authors in [32] derive the joint uplink/downlink coverage probability as the product of two coverage probabilities. For more accurate analysis, one should of course capture this correlation explicitly, as done in [33], where the authors provided the accurate joint distribution of uplink and downlink pathloss for generalized uplink/downlink cell association policies (associating with the same BS in both channels is a special case). Assuming independent interference levels over uplink and downlink channels, they use this joint distribution to derive the joint uplink/downlink coverage.

In this paper we study the performance of *on-the-fly* reception/transmission in a cellular-based IoT network where the IoT devices first harvest energy and then use it to receive/transmit information in the same time slot. Assuming cellular transmissions to be the only source of RF energy for

[1]Throughput this paper, we will refer to the IoT networks in which the IoT devices have uninterrupted access to a reliable energy source, such as power grid or a battery, as the regularly powered networks.

the IoT devices, we study the joint probability of a typical IoT device harvesting sufficient energy *and* achieving both uplink and downlink SINR thresholds with respect to its associated base station in a given time slot. As noted already, we will refer to this as *uplink/downlink coverage probability* in this paper. Since the same infrastructure (cellular BSs) is used for charging and communication, there is inherent correlation in the energy and uplink/downlink coverage events, which is carefully incorporated in our analysis. Please refer to Section II for more details on the system setup. We now summarize the contributions of this paper.

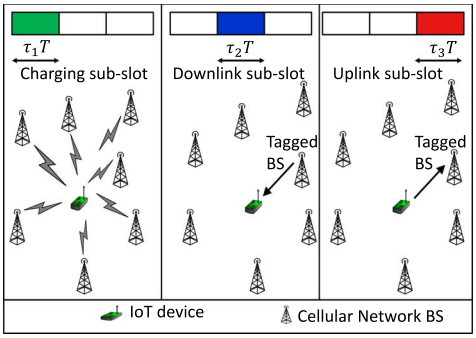

Fig. 1. Illustration of the system setup and the three sub-slots (charging, downlink, and uplink).

B. Contributions and Outcomes

Cellular-based IoT model: We develop a comprehensive model for cellular-based RF-powered IoT network in which the locations of the BSs and the IoT devices are modeled using two independent Poisson point processes (PPPs). Each time slot is assumed to be partitioned into three sub-slots: (i) *charging sub-slot*, in which the received power from the cellular network is used for charging devices to enable them to perform information transmission/reception in the next two sub-slots, (ii) *downlink sub-slot*, in which the devices receive information from their associated BSs, and (iii) *uplink sub-slot*, in which the devices transmit information to their associated BSs using *fractional* channel inversion power control. Contrary to the prior works discussed above that focused on the separate analysis of uplink and downlink coverage, in this paper we focus on the analysis of joint uplink/downlink coverage (defined as the joint probability of energy coverage, uplink SINR coverage, and downlink SINR coverage). Since cellular network is assumed to be the only source of RF energy for the IoT devices, the energy and uplink/downlink coverage events are tightly coupled through the locations of the cellular BSs. In particular, the amount of energy harvested by each device is highly correlated with both the uplink and downlink SINR achieved by that device. Naturally, the uplink and downlink coverage events are also coupled. As discussed next, we carefully handle this correlation in our analysis, which is also one of the main technical contributions of this paper.

Joint uplink/downlink coverage analysis: As stated already, we define joint uplink/downlink coverage as the joint probability that the typical device harvests sufficient energy in the first sub-slot, achieves high enough downlink SINR in the second sub-slot, and achieves high enough uplink SINR in the third sub-slot. These three events are correlated because of their dependence on the point processes modeling the devices and the base stations. That being said, if we assume independent fading across the three sub-slots and condition on the point processes, the three events become *conditionally* independent. We therefore, derive the conditional probabilities of the three events first. The complexity of this problem should be evident from the following two facts: (i) the exact characterization of uplink SINR in a conventional single-tier cellular setup is not known in the stochastic geometry literature [13], and (ii) the total energy harvested is essentially a power-law shot noise process whose probability distribution function is not known in general. On top of these challenges, we need to jointly decondition (average) over the point processes in order to obtain the joint uplink/downlink coverage, which adds to the complexity of the problem. We overcome all these challenges by developing a dominant BS-based approximation approach that not only provides a tight approximation for the power-law shot noise process (energy harvested) but also facilitates joint deconditioning over the point processes. The tightness of the approximate joint coverage expression is verified by comparing it with the simulation results.

Useful system insights: Our analytical results provide several useful system insights. First, we demonstrate the existence of optimal time-slot partitioning that maximizes system throughput. The effect of other system parameters on this optimal partitioning is studied numerically. We then compare the performance of the RF-powered IoT system with the one in which IoT devices have access to a reliable power source (termed regularly powered network). Our analytical results reveal several interesting thresholds beyond which the performance of this RF-powered network is similar to that of the regularly powered network. For instance, we show that if the distance of the typical device to the second closest BS is below a certain threshold, its downlink coverage performance would be the same as the regularly powered network. We further study the effect of other system parameters including time-slot partitioning parameters, cellular network density, RF-DC conversion efficiency, and cellular network transmission power on the system performance. We show how these parameters can be tuned in order to get the performance of this RF-powered network closer to that of a regularly powered network. This is done by defining a *tuning parameter* that captures the effect of the aforementioned system parameters. Our analysis shows that in order to get the performance of this RF-powered network closer to the regularly powered network, it is only required to make sure that this tuning parameter is large enough.

II. System Model

We consider a cellular-based IoT network in which the IoT devices are solely powered by the ambient RF energy. In this work, we assume that the cellular transmissions are the only source of ambient RF energy for these devices. Quite reasonably, the IoT devices are assumed to be batteryless (similar

to [34] and [35]). The more general case of finite-sized battery is left for future work. In particular, we assume that all the energy required for uplink and/or downlink communication by a device in a given time slot will need to be harvested by that device in the same time slot.[2] More details will be provided shortly. The locations of the cellular network BSs and the IoT devices are modeled by two independent PPPs $\Phi_b \equiv \{x_i\} \subset \mathbb{R}^2$ and $\Phi_u \equiv \{u_i\} \subset \mathbb{R}^2$ with densities λ_b and λ_u, respectively [36]. As will be the case in reality, we assume $\lambda_u > \lambda_b$.

As implied in Fig. 1, we assume that each IoT device adopts the time-switching receiver architecture (see [10]) in which the antenna is used for energy harvesting for a given fraction of time and for communication for the rest of the time. The time slot duration is assumed to be T (seconds). As shown in Fig. 1, each time-slot is further divided into charging, downlink, and uplink sub-slots with durations $T_{\text{ch}} = \tau_1 T$, $T_{\text{tr}}^{\text{DL}} = \tau_2 T$, and $T_{\text{tr}}^{\text{UL}} = \tau_3 T$, respectively. During the *charging sub-slot*, all the BSs in the network act as RF chargers for the IoT devices. In the downlink and uplink sub-slots, each IoT device receives and sends information to its associated BS, respectively.[3] This system setup will facilitate the analysis of joint uplink/downlink coverage probability thus generalizing the prior work on energy harvesting networks that focused on the analysis of downlink and uplink separately. Naturally, if we substitute $\tau_2 = 0$, we can focus only on the uplink analysis, which we refer to as the *uplink mode*. Similarly, if we substitute $\tau_3 = 0$, we can focus only on the downlink analysis, which we refer to as the *downlink mode*. The general case in which τ_2 and τ_3 are both non-zero will be referred to as the *joint uplink/downlink mode*. Our analysis will be performed under the following assumptions: (i) each IoT device connects to its *nearest* BS (referred to as *tagged* BS in the rest of the paper), (ii) fading gains across all links are independent, (iii) fading gains across the same link in charging sub-slot (denoted by g_x), downlink sub-slot (denoted by h_x), and uplink sub-slot (denoted by w_x) are independent, (iv) all channels suffer from Rayleigh fading. This means that g_x, h_x, and w_x are all independent exponential random variables with mean 1. Under these assumptions, we focus our analysis on a typical device placed at the origin (without loss of generality due to the stationarity of PPP). We now enrich our notation to express key metrics of interest for each sub-slot.

In the charging sub-slot, we are interested in measuring the amount of energy harvested by the typical device. In order to do that, we first model the received power at the typical device from a BS located at $x \in \Phi_b$ as $P_{\text{t}} g_x \|x\|^{-\alpha}$, where $g_x \sim \exp(1)$ is the fading gain, P_{t} is the transmission power (assumed to be the same for all the BSs), and $\|x\|^{-\alpha}$ models standard power law path-loss with exponent $\alpha > 2$ (assumed to be the same for all the links in the network). Multi-slope path-loss model capturing the distance-dependence in the value of path-loss exponent, e.g., [38], is left for future work. The total energy harvested by the typical device is thus

$$E_{\text{H}} = \tau_1 T \eta \sum_{x \in \Phi_b} P_{\text{t}} g_x \|x\|^{-\alpha} \text{ Joules}, \tag{1}$$

where $\eta < 1$ represents the efficiency of the RF-to-DC conversion.

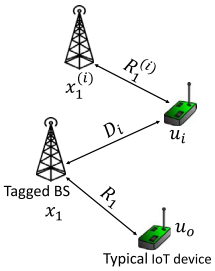

Fig. 2. Key variables used in the uplink analysis.

In the downlink and uplink sub-slots, we are interested in the expressions for the respective SINRs. For the downlink sub-slot, the SINR at the typical device is

$$\text{SINR}_{\text{DL}} = \frac{P_{\text{t}} h_{x_1} \|x_1\|^{-\alpha}}{\sum_{x \in \Phi_b \setminus x_1} P_{\text{t}} h_x \|x\|^{-\alpha} + \sigma_{\text{DL}}^2} = \frac{P_{\text{t}} h_{x_1} \|x_1\|^{-\alpha}}{I_1 + \sigma_{\text{DL}}^2}, \tag{2}$$

where $h_x \sim \exp(1)$ represents the fading gain between the typical device and the BS located at x, x_1 is the location of the nearest (tagged) BS, I_1 denotes the interference power, and σ_{DL}^2 models thermal noise power. For successful reception in the downlink sub-slot, the received SINR needs to be greater than a modulation-and-coding specific target SINR β_{DL}. In addition, the IoT device needs a minimum amount of energy $\mathcal{E}(\tilde{R}, \tau_2)$ in order to be able to receive data successfully during the downlink sub-slot, where $\tilde{R} = \log_2(1 + \beta_{\text{DL}})$. The function $\mathcal{E}(\tilde{R}, \tau_2)$ is a linear function of τ_2 and a convex function of $\tilde{R}$. This model is commonly used in literature as discussed in [39] and the references therein.

In the uplink sub-slot, each IoT device is assumed to perform uplink fractional channel inversion power control. Hence, if the distance between the IoT device and its serving BS is R, then the transmitted power is $\rho R^{\epsilon\alpha}$, where ρ is the BS sensitivity, and $\epsilon \in [0, 1]$ is the power control parameter. Therefore, the typical IoT device requires $\tau_3 T \rho R^{\epsilon\alpha}$ energy in order to perform uplink transmission. We refer to IoT devices that have enough energy to transmit in the uplink sub-slot as *active* devices. Focusing our analysis on the typical device located at the origin, the uplink SINR for this device measured at its tagged BS is:

$$\text{SINR}_{\text{UL}} = \frac{w_o \rho \|x_1\|^{(\epsilon-1)\alpha}}{\sum\limits_{u_i \in \Phi_a \setminus u_o} \delta_i w_i \rho \left(R_1^{(i)}\right)^{\epsilon\alpha} D_i^{-\alpha} + \sigma_{\text{UL}}^2}, \tag{3}$$

where Φ_a is the point process representing all the devices (including the typical device) that are scheduled on the same time-frequency resource as the typical device, σ_{UL}^2 models

[2]The IoT device uses a supercapacitor to store the harvested energy. The large charging and discharging rates of the supercapacitor enable using the harvested energy during the same time-slot. However, due to supercapacitor's relatively large leakage current, any unused energy remaining by the end of the time-slot is assumed to be unavailable for use during the next time-slot.

[3]We assume that there is perfect synchronization across all BSs and the IoT devices, which is quite reasonable in a cellular-based IoT network. For instance, this can be easily achieved by using the 3GPP NB-IoT technology [37].

thermal noise power, $w_i \sim \exp(1)$ is the channel fading gain between the device located at u_i and the tagged BS during uplink information sub-slot, x_1 is the location of the tagged BS, $D_i = \|u_i - x_1\|$ is the distance between the device located at u_i and the tagged BS, $R_1^{(i)}$ is the distance between the device located at u_i and its serving BS (which is the closest BS to this device by definition), and u_o is the location of the typical device. Also δ_i is an indicator function that equals to 1 if the IoT device located at u_i is *active*, and 0 otherwise. Please refer to Fig. 2 for the summary of this uplink-specific notation. As was the case in downlink, this SINR needs to be greater than a modulation-and-coding specific target SINR threshold β_{UL} for successful transmission.

Joint uplink/downlink coverage: With this, we are now ready to formally introduce the key metric of interest for this paper: the joint uplink/downlink coverage probability. Recall that the total energy harvested by a device in the charging sub-slot is used by that device to receive information from the tagged BS during the downlink sub-slot and transmit information to the tagged BS during the uplink sub-slot. Hence, the energy coverage condition for this case is:

$$E_{\mathrm{H}} \geq E_{\min}, \tag{4}$$

where $E_{\min} = \mathcal{E}(\tilde{R}, \tau_2) + \tau_3 T \rho r_1^{\epsilon\alpha}$, $r_1 = \|x_1\|$ is the distance between the typical IoT device and its nearest BS. For completeness, three conditions need to be satisfied for uplink/downlink coverage: (i) $E_{\mathrm{H}} > E_{\min}$, (ii) $\mathrm{SINR}_{\mathrm{DL}} > \beta_{\mathrm{DL}}$ in the downlink sub-slot, and (iii) $\mathrm{SINR}_{\mathrm{UL}} > \beta_{\mathrm{UL}}$ in the uplink sub-slot. Therefore, the joint uplink/downlink coverage probability is defined as $P_{\mathrm{suc}}^{\mathrm{J}} =$

$$\mathbb{E}[\mathbb{1}(\mathrm{SINR}_{\mathrm{DL}} \geq \beta_{\mathrm{DL}})\mathbb{1}(\mathrm{SINR}_{\mathrm{UL}} \geq \beta_{\mathrm{UL}})\mathbb{1}(E_{\mathrm{H}} \geq E_{\min})]. \tag{5}$$

As noted already, when τ_2 and τ_3 are both non-zero, we call this a *joint uplink/downlink mode*. As discussed next, if one of them is zero, we can specialize the above definition of joint coverage to study downlink or uplink coverage probability separately.

Downlink coverage: If we substitute $\tau_3 = 0$, each time slot is partitioned into charging and downlink sub-slots. We referred to this as the *downlink mode* above. Since each device in this mode only needs to perform downlink transmission, the energy coverage condition reduces to $E_{\mathrm{H}} > \mathcal{E}(\tilde{R}, \tau_2)$. Consequently, the downlink coverage probability for this case can be defined as:

$$P_{\mathrm{cov}}^{\mathrm{DL}} = \mathbb{E}\big[\mathbb{1}(\mathrm{SINR}_{\mathrm{DL}} \geq \beta_{\mathrm{DL}})\mathbb{1}\big(E_{\mathrm{H}} \geq \mathcal{E}\big(\tilde{R}, \tau_2\big)\big)\big]. \tag{6}$$

If $\mathrm{SINR}_{\mathrm{DL}} \geq \beta_{\mathrm{DL}}$ and $E_{\mathrm{H}} \geq \mathcal{E}(\tilde{R}, \tau_2)$ (i.e., the IoT device is able to establish a communication link with the BS), the downlink data rate is $R = W_D \log(1 + \beta_{\mathrm{DL}})$ bps in the information sub-slot, where W_D is the bandwidth of the downlink channel.

Uplink coverage: Similarly, if we substitute $\tau_2 = 0$, there is no downlink sub-slot and each time slot is partitioned into only charging and uplink sub-slots. This was referred to as the *uplink mode* earlier in this section. Since each IoT device now needs to perform only uplink communication, the energy coverage condition for this case is $E_{\mathrm{H}} > \tau_3 T \rho R^{\epsilon\alpha}$. This along with the uplink SINR coverage condition gives the following definition for the uplink coverage probability:

$$P_{\mathrm{suc}}^{\mathrm{UL}} = \mathbb{E}\big[\mathbb{1}(\mathrm{SINR}_{\mathrm{UL}} \geq \beta_{\mathrm{UL}})\mathbb{1}\big(E_{\mathrm{H}} \geq \tau_3 T \rho r_1^{\epsilon\alpha}\big)\big]. \tag{7}$$

If the two coverage conditions ($\mathrm{SINR}_{\mathrm{UL}} \geq \beta_{\mathrm{UL}}$ and $E_{\mathrm{H}} \geq \tau_3 T \rho r_1^{\epsilon\alpha}$) are satisfied, the uplink data rate is $R = W_U \log(1 + \beta_{\mathrm{UL}})$ bps in the information sub-slot, where W_U is the bandwidth of the uplink channel.

As evident from the above discussion, joint uplink/downlink coverage probability encompasses the other two as special cases. We will therefore start with the analysis of this general case. The results for the downlink and uplink modes will be provided as special cases of this general setup to provide useful system design insights.

III. Joint Uplink and Downlink Mode

This is the first technical section of the paper in which we will evaluate the joint uplink/downlink coverage probability defined in (5). In particular, our goal is to evaluate the joint probability of the following three events: (i) $\mathrm{SINR}_{\mathrm{DL}} \geq \beta_{\mathrm{DL}}$, (ii) $\mathrm{SINR}_{\mathrm{UL}} \geq \beta_{\mathrm{UL}}$, and (iii) $E_{\mathrm{H}} \geq E_{\min}$. Keeping the joint treatment aside, the complexity of this analysis should be evident from the following two facts: (i) the exact characterization of $\mathbb{P}(\mathrm{SINR}_{\mathrm{UL}} \geq \beta_{\mathrm{UL}})$ is not known in the stochastic geometry literature [13], [40], and (ii) the total energy harvested is essentially a power-law shot noise process whose probability density function is not known in general. To make matters worse, all these events depend upon the point process Φ_b modeling the locations of the BSs, which necessitates their joint analysis. This dependence on Φ_b is quite evident for both E_{H} and $\mathrm{SINR}_{\mathrm{DL}}$ from their expressions given by Eqs. (1) and (2). While $\mathrm{SINR}_{\mathrm{UL}}$ may not appear to depend on Φ_b on the first look (see (3)), the point processes of the devices and BSs are correlated through cell selection and resource scheduling (see [13] for the detailed discussion), which couples the uplink coverage event with the other two events. Therefore, the main challenge in our analysis is the joint treatment of these three coverage events. That being said, since the main source of this correlation, as evident from Eqs. (1), (2), (3), is the dependence of the three events on Φ_b, they can be treated as independent when conditioned on Φ_b since the fading gains (h_x, g_x, and w_x) in the three sub-slots are assumed independent. Consequently, the joint uplink/downlink coverage probability defined in (5) can be expressed as

$$P_{\mathrm{suc}}^{\mathrm{J}} = \mathbb{E}_{\Phi_b}[\mathbb{P}(\mathrm{SINR}_{\mathrm{DL}} \geq \beta_{\mathrm{DL}}|\Phi_b)\mathbb{P}(\mathrm{SINR}_{\mathrm{UL}} \geq \beta_{\mathrm{UL}}|\Phi_b) \times \mathbb{P}(E_{\mathrm{H}} \geq E_{\min}|\Phi_b)]. \tag{8}$$

In the following subsections, we carefully approximate the three conditional probability terms using a dominant BS-based approach. The resulting expressions will then be used to derive our main result for the joint uplink/downlink coverage probability in Theorem 1.

A. Conditional Energy Coverage Probability

As discussed above, $\mathrm{SINR}_{\mathrm{DL}}$ and E_{H} both depend upon Φ_b explicitly. However, due to pathloss, the BSs located far away from the typical device do not contribute as much to

TABLE I
TABLE OF NOTATIONS

Notation	Description
Φ_b; λ_b	PPP modeling the locations of BSs in the cellular network; density of the BSs
Φ_u; λ_u	PPP modeling the locations of IoT devices; density of the IoT devices
τ_1; τ_2; τ_3	Time-slot division parameter for charging sub-slot; downlink sub-slot; uplink sub-slot
E_{H}	Amount of energy harvested from ambient RF signals (in Joules)
D_{avg}	Average data rate (throughput)
$P_{\mathrm{cov}}^{\mathrm{DL,RP}}$; $P_{\mathrm{suc}}^{\mathrm{UL,RP}}$	Downlink coverage probability; uplink coverage probability in a regularly powered network
$P_{\mathrm{cov}}^{\mathrm{DL}}$; $P_{\mathrm{suc}}^{\mathrm{UL}}$; $P_{\mathrm{suc}}^{\mathrm{J}}$	Downlink coverage probability; uplink coverage probability; joint uplink/downlink coverage probability in the ambient RF powered network
g_x; h_x; w_x	Fading gains during charging; downlink; uplink sub-slots (assumed to be i.i.d. across all links). Rayleigh fading is assumed
W_D (W_U)	Bandwidth of the downlink channel (uplink channel)
P_{t}; ρ	BS transmission power; BS sensitivity
ϵ; α	Power control parameter; path loss exponent ($\alpha > 2$)
r_1 (r_2)	Distance between typical IoT device and its nearest BS (2nd nearest BS)

both these terms as the BSs located close to the typical point. Therefore, we reduce the dimensionality of this problem by considering the effect of closest two BSs to the typical device exactly and approximating the effect of the rest of the BSs. It will be clear shortly why we chose two and not any other number. This dominant BS-based approach is useful when the exact analysis is either too difficult or leads to unwieldy results. It has been used in the past to analyze the coverage of ad hoc networks [41], coverage of downlink cellular networks [42], k-coverage of localization networks [43], [44], and downlink coverage of wireless networks of unmanned aerial vehicles [45], [46]. Since all these works focused on some form of (marginal) SINR-based coverage, they are not applicable to our analysis because of the need to perform conditional analysis of each term separately and then decondition jointly over all the terms. These works are listed here mainly for completeness. Another main difference between these works and ours is that the dominant BS approach is only used to approximate the interference in the SINR term, while in our case it is also used to approximate the overall amount of energy harvested by the IoT device.

We apply this approach to approximate the total energy harvested by the typical device in the charging sub-slot (given by (1)) by the energy harvested from the nearest two BSs (located at distances $r_1 = \|x_1\|$ and $r_2 = \|x_2\|$ from the typical device) and the conditional mean (conditioned on the location of the nearest 2 BSs) of the rest of the terms as follows:

$$E_{\mathrm{H}} = \tau_1 T \eta P_{\mathrm{t}} \sum_{x \in \Phi_b} g_x \|x\|^{-\alpha} \approx \tau_1 T \eta P_{\mathrm{t}} \big(g_{x_1} \|x_1\|^{-\alpha} + g_{x_2} \|x_2\|^{-\alpha} + \Psi(r_2) \big), \quad (9)$$

where $\Psi(r_2) = \mathbb{E}[\sum_{x \in \Phi_b \setminus x_1, x_2} g_x \|x\|^{-\alpha} | x_1, x_2]$. We will use this approximation to compute the conditioned energy coverage probability $\mathbb{P}(E_H \geq \mathbb{E}_{\min} | \Phi_b)$ which is necessary for the computation of $P_{\mathrm{suc}}^{\mathrm{J}}$ as explained above. In addition to enabling the joint coverage analysis, this approximation will also lead to several crisp system design insights. For instance, as a result of using this approximation, we will be able to define a threshold on r_2 (as well as λ_b and time switching parameters) below which the performance is approximately equivalent to that of a regularly powered cellular-based IoT (further discussion will be provided in Remarks 5 and 8). As discussed already, the typical IoT device needs to harvest a minimum amount of energy $E_{\min} = \mathcal{E}(\tilde{R}, \tau_2) + \tau_3 T \rho \|x_1\|^{\epsilon \alpha}$ to be able to receive and transmit information. If it is able to harvest this energy, it is said to be in *energy coverage*. In the following Lemma we derive an expression for the conditional energy coverage probability using the approximation in (9).

Lemma 1 (Conditional Energy Coverage Probability): Probability that the harvested energy during the charging sub-slot is greater than $E_{\min}$ conditioned on the point process Φ_b is

$$\mathbb{P}(E_{\mathrm{H}} \geq E_{\min} | \Phi_b) = \frac{r_2^{\alpha} \exp\big(-r_1^{\alpha} [\mathcal{F}(r_1, r_2)]^{+}\big)}{r_2^{\alpha} - r_1^{\alpha}} - \frac{r_1^{\alpha} \exp\big(-r_2^{\alpha} [\mathcal{F}(r_1, r_2)]^{+}\big)}{r_2^{\alpha} - r_1^{\alpha}}, \quad (10)$$

while the unconditioned probability is

$$\mathbb{P}(E_{\mathrm{H}} \geq E_{\min}) = \int_0^{\infty} \int_{r_1 \in \mathcal{N}_{r_2}} f_{R_1, R_2}(r_1, r_2) \mathrm{d}r_1 \mathrm{d}r_2 + \int_0^{\infty} \int_{r_1 \in \mathcal{P}_{r_2}} f_{R_1, R_2}(r_1, r_2) \left(\frac{r_2^{\alpha} \exp\big(-r_1^{\alpha} [\mathcal{F}(r_1, r_2)]^{+}\big)}{r_2^{\alpha} - r_1^{\alpha}} - \frac{r_1^{\alpha} \exp\big(-r_2^{\alpha} [\mathcal{F}(r_1, r_2)]^{+}\big)}{r_2^{\alpha} - r_1^{\alpha}} \right) \mathrm{d}r_1 \mathrm{d}r_2, \quad (11)$$

where $\mathcal{F}(r_1, r_2) = [C(\tau_1) + \frac{\tau_3 \rho r_1^{\epsilon \alpha}}{\tau_1 \eta P_{\mathrm{t}}} - \frac{2\pi \lambda_b}{\alpha - 2} r_2^{2-\alpha}]$, $C(\tau_1) = \frac{\mathcal{E}(\tilde{R}, \tau_2)}{\tau_1 T \eta P_{\mathrm{t}}}$, $[x]^{+} = \max\{0, x\}$, $f_{R_1, R_2}(r_1, r_2) = (2\pi\lambda_b)^2 r_1 r_2 e^{-\lambda_b \pi r_2^2}$, $\mathcal{N}_{r_2} = \{r_1 : \mathcal{F}(r_1, r_2) \leq 0,\ r_1 < r_2\}$, and $\mathcal{P}_{r_2} = \{r_1 : \mathcal{F}(r_1, r_2) \geq 0,\ r_1 < r_2\}$.

Proof: See Appendix A. ∎

As explained before, the above expression can be used to compute the energy coverage probability in the downlink mode by eliminating uplink conditions and vice versa for the uplink mode. The complete results for these special cases will be presented in Lemmas 4 and 5.

B. Conditional SINR Coverage Probability

As a result of using the approximation introduced in (9), the conditional energy coverage probability in (10) is only a function of the distances r_1 and r_2 (between the typical device and its nearest two BSs). Keeping in mind that we will have to jointly decondition on all the coverage events at the end (as evident from (8)), it will be useful to derive conditional downlink SINR coverage also in terms of r_1 and r_2. In order to do that, we use the same dominant BS-based approach that we used in the previous subsection. In particular, we approximate the interference in the denominator of SINR in (2) by the interference from the second nearest BS (strongest interferer) and the expectation of the interference from the rest of the BSs. Under this approximation, the conditional downlink SINR coverage probability becomes $\mathbb{P}(\mathrm{SINR}_{\mathrm{DL}} \geq \beta_{\mathrm{DL}} | r_1, r_2)$. A tractable expression for this conditional probability is derived next.

Lemma 2 (Conditional Downlink SINR Coverage Probability): Probability that the downlink SINR at the typical device exceeds β_{DL}, conditioned on r_1 and r_2, is

$$\mathbb{P}(\mathrm{SINR}_{\mathrm{DL}} \geq \beta_{\mathrm{DL}} | r_1, r_2) = \exp\big(-\mathcal{G}(r_1, r_2)\big) \frac{1}{1 + \frac{\beta_{\mathrm{DL}} r_1^{\alpha}}{r_2^{\alpha}}}, \tag{12}$$

where $\mathcal{G}(r_1, r_2) = \frac{\beta_{\mathrm{DL}} \sigma_{\mathrm{DL}}^2 r_1^{\alpha}}{P_{\mathrm{t}}} + \frac{2\pi\lambda_b \beta_{\mathrm{DL}} r_1^{\alpha}}{(\alpha-2) r_2^{\alpha-2}}$.

Proof: See Appendix B. ∎

With this, we are now left with deriving the conditional uplink probability, which we do next. It is noteworthy that uplink analysis is known to be a challenging problem even for regularly powered networks. The locations of the devices scheduled in the same time frequency resource block as the typical device (modeled as point process $\Phi_a \backslash u_o$ in (3)) are correlated with the locations of the BSs due to the structure of the Poisson Voronoi tessellation. This correlation is further enhanced due to uplink power control, where the transmission power of each device is a function of its distance to its serving BS. As discussed in [13], the exact analysis of this setup in not known. It has, however, been shown that modeling the locations of the devices by an independent PPP and handling dependence between the distances D_i and $R_1^{(i)}$ (as defined in (3)) appropriately leads to a fairly tight approximation. For the latter, it is sufficient to just account for the fact that $R_1^{(i)} < D_i$, i.e., the serving BS must be closer to the interfering device than the tagged BS. Please refer to [13] for more details. Using this general idea, the Laplace transform of the aggregate interference $I_2 = \sum_{u_i \in \Phi_a \backslash u_o} w_i (R_1^{(i)})^{\epsilon\alpha} D_i^{-\alpha}$ at the tagged BS in a regularly powered network was given in [13] as follows:

$$\mathcal{L}_{I_2}(s) = \mathbb{E}\big[e^{-I_2 s}\big] = \exp\Bigg(-2\pi\lambda_b \times \int_0^{\infty} \int_0^{x^2} \frac{1}{1 + (s)^{-1} u^{-\alpha\epsilon/2} x^{\alpha}} \pi \lambda_b e^{-\lambda_b \pi u} \mathrm{d}u x \mathrm{d}x \Bigg), \tag{13}$$

where Φ_a is the point process modeling the locations of the selected devices in a given time-frequency resource. This expression was used to derive the uplink coverage probability for regularly powered networks in [13] as follows:

$$P_{\mathrm{suc}}^{\mathrm{UL,RP}} = \int_0^{\infty} f_{R_1}(r_1) e^{\left(-\frac{\beta_{\mathrm{UL}} \sigma_{\mathrm{UL}}^2}{\rho r_1^{(\epsilon-1)\alpha}}\right)} \mathcal{L}_{I_2}\left(\frac{\beta_{\mathrm{UL}}}{r_1^{(\epsilon-1)\alpha}}\right) \mathrm{d}r_1, \tag{14}$$

where $f_{R_1}(r_1) = 2\pi\lambda_b r_1 \exp(-\pi\lambda_b r_1^2)$. We will use this expression to compare the performance of the proposed setup to that of the regularly powered networks.

Coming to the conditional uplink coverage in the proposed energy harvesting setup, note that the dominant source of correlation between uplink SINR and the other two terms (downlink SINR and the amount of energy harvested) is the serving distance r_1. If we condition on r_1 and treat Φ_a and Φ_b as independent point processes (as done above), the conditional uplink coverage probability reduces to $\mathbb{P}(\mathrm{SINR}_{\mathrm{UL}} \geq \beta_{\mathrm{UL}} \big| r_1)$, which is derived in the next Lemma.

Lemma 3 (Conditional Uplink SINR Coverage Probability): Probability that the uplink SINR of the typical device at the tagged BS is greater than β_{UL}, conditioned on r_1, is

$$\mathbb{P}\Big(\mathrm{SINR}_{\mathrm{UL}} \geq \beta_{\mathrm{UL}} \Big| r_1\Big) = e^{\left(-\frac{\beta_{\mathrm{UL}} \sigma_{\mathrm{UL}}^2}{\rho r_1^{(\epsilon-1)\alpha}}\right)} \mathcal{L}_{\tilde{I}_2}\left(\frac{\beta_{\mathrm{UL}}}{r_1^{(\epsilon-1)\alpha}}\right), \tag{15}$$

where $\mathcal{L}_{\tilde{I}_2}(s)$ is given by (13) by replacing λ_b with $\tilde{\lambda}_b = P_h \lambda_b$, where $P_h = \mathbb{P}(E_{\mathrm{H}} \geq E_{\min})$.

Proof: See Appendix B. ∎

C. Joint Uplink/Downlink Coverage Probability

Having derived the three conditional probability terms appearing in (8) in Lemmas 1, 2, and 3, we are now ready to derive the joint uplink/downlink coverage probability. The only remaining step is to uncondition their product with respect to the joint distribution of r_1 and r_2, which results in the following Theorem.

Theorem 1 (Joint Uplink/Downlink Coverage Probability): The joint uplink/ downlink coverage probability $P_{\mathrm{suc}}^{\mathrm{J}}$ of the typical IoT device with downlink and uplink SINR thresholds β_{DL} and β_{UL} respectively is given by:

$$\begin{aligned} P_{\mathrm{suc}}^{\mathrm{J}} = & \int_0^{\infty} \int_{r_1 \in \mathcal{N}_{r_2}} f_{R_1,R_2}(r_1, r_2) e^{\left(-\frac{\beta_{\mathrm{UL}} \sigma_{\mathrm{UL}}^2}{\rho r_1^{(\epsilon-1)\alpha}}\right)} \mathcal{L}_{\tilde{I}_2}\left(\frac{\beta_{\mathrm{UL}}}{r_1^{(\epsilon-1)\alpha}}\right) \\ & \times \exp\big(-\mathcal{G}(r_1, r_2)\big) \frac{1}{1 + \frac{\beta_{\mathrm{DL}} r_1^{\alpha}}{r_2^{\alpha}}} \mathrm{d}r_1 \mathrm{d}r_2 \\ & + \int_0^{\infty} \int_{r_1 \in \mathcal{P}_{r_2}} f_{R_1,R_2}(r_1, r_2) e^{\left(-\frac{\beta_{\mathrm{UL}} \sigma_{\mathrm{UL}}^2}{\rho r_1^{(\epsilon-1)\alpha}}\right)} \mathcal{L}_{\tilde{I}_2}\left(\frac{\beta_{\mathrm{UL}}}{r_1^{(\epsilon-1)\alpha}}\right) \\ & \times \frac{\exp\big(-\mathcal{G}(r_1, r_2) - r_1^{\alpha} \mathcal{F}(r_1, r_2)\big)}{r_2^{\alpha} - r_1^{\alpha}} \frac{r_2^{\alpha}}{1 + \frac{\beta_{\mathrm{DL}} r_1^{\alpha}}{r_2^{\alpha}}} \mathrm{d}r_1 \mathrm{d}r_2 \\ & - \int_0^{\infty} \int_{r_1 \in \mathcal{P}_{r_2}} f_{R_1,R_2}(r_1, r_2) e^{\left(-\frac{\beta_{\mathrm{UL}} \sigma_{\mathrm{UL}}^2}{\rho r_1^{(\epsilon-1)\alpha}}\right)} \mathcal{L}_{\tilde{I}_2}\left(\frac{\beta_{\mathrm{UL}}}{r_1^{(\epsilon-1)\alpha}}\right) \\ & \times \frac{\exp\big(-\mathcal{G}(r_1, r_2) - r_2^{\alpha} \mathcal{F}(r_1, r_2)\big)}{r_2^{\alpha} - r_1^{\alpha}} \frac{r_1^{\alpha}}{1 + \frac{\beta_{\mathrm{DL}} r_1^{\alpha}}{r_2^{\alpha}}} \mathrm{d}r_1 \mathrm{d}r_2, \end{aligned} \tag{16}$$

where $f_{R_1,R_2}(r_1,r_2) = (2\pi\lambda_b)^2 r_1 r_2 e^{-\pi\lambda_b r_2^2}$, $\mathcal{F}(r_1,r_2)$, $\mathcal{N}_{r_2}$, $\mathcal{P}_{r_2}$ are as introduced in Lemma 1, $\mathcal{G}(r_1,r_2)$ is as introduced in Lemma 2, and $\mathcal{L}_{\tilde{I}_2}(s)$ is as introduced in Lemma 3.

Proof: This result follows directly by substituting (10), (12), (15) in (8) and integrating over r_1 and r_2 using the joint distribution $f_{R_1,R_2}(r_1,r_2)$ as defined in [47, eq. (28)]. ∎

Remark 1: This general result can be used to derive both downlink coverage and uplink coverage probabilities defined in Eqs. (6) and (7). For instance, if we remove all the uplink conditions by putting $\beta_{\mathrm{UL}} = 0$ (note that $\mathcal{L}_{I_2}(0) = 1$) and $\tau_3 = 0$, then (16) will represent the downlink coverage probability P_{cov}^{DL} for the downlink mode. Similarly, if we remove all the downlink conditions by putting $\beta_{\mathrm{DL}} = 0$ (note that $\mathcal{G}(r_1,r_2) = 0$ in that case), $\mathcal{E}(\tilde{R},\tau_2) = 0$, and $\tau_2 = 0$, then (16) will represent the uplink coverage probability $P_{\mathrm{suc}}^{\mathrm{UL}}$ for the uplink mode.

D. Average Throughput

We now derive expressions for both the uplink and the downlink average throughput in the joint uplink/downlink mode. The average downlink throughput is

$$\begin{aligned} D_{\mathrm{avg}}^{\mathrm{DL}} = \tau_2 R_{\mathrm{avg}}^{\mathrm{DL}} &= \tau_2 \mathbb{E}\big[W_D \log(1+\beta_{\mathrm{DL}})\mathbb{1}(\mathrm{SINR}_{\mathrm{DL}} \geq \beta_{\mathrm{DL}}) \\ &\quad \times \mathbb{1}(\mathrm{SINR}_{\mathrm{UL}} \geq \beta_{\mathrm{UL}})\mathbb{1}(E_{\mathrm{H}} \geq E_{\min})\big] \\ &= \tau_2 W_D \log(1+\beta_{\mathrm{DL}}) P_{\mathrm{suc}}^{\mathrm{J}}, \end{aligned} \tag{17}$$

where $R_{\mathrm{avg}}^{\mathrm{DL}}$ is the average data rate during downlink sub-slot in the joint mode. The multiplication by τ_2 accounts for the fact that downlink sub-slot lasts for τ_2 fraction of the total time-slot duration. Similarly, the average uplink throughput in the joint mode is:

$$\begin{aligned} D_{\mathrm{avg}}^{\mathrm{UL}} = \tau_3 R_{\mathrm{avg}}^{\mathrm{UL}} &= \tau_3 \mathbb{E}\big[W_U \log(1+\beta_{\mathrm{UL}})\mathbb{1}(\mathrm{SINR}_{\mathrm{UL}} \geq \beta_{\mathrm{UL}}) \\ &\quad \times \mathbb{1}(\mathrm{SINR}_{\mathrm{DL}} \geq \beta_{\mathrm{DL}}) \times \mathbb{1}(E_{\mathrm{H}} \geq E_{\min})\big] \\ &= \tau_3 W_U \log(1+\beta_{\mathrm{UL}}) P_{\mathrm{suc}}^{\mathrm{J}}, \end{aligned} \tag{18}$$

where $R_{\mathrm{avg}}^{\mathrm{UL}}$ is the average data rate during uplink sub-slot in the joint mode.

Remark 2: Note that for a given τ_3, it is easier to satisfy the energy constraint for larger values of τ_1. This means both $P_{\mathrm{suc}}^{\mathrm{J}}$ and $R_{\mathrm{avg}}^{\mathrm{DL}}$ are increasing functions of τ_1. However, increasing τ_1 decreases τ_2 (for a given τ_3), which reduces the downlink transmission time and may therefore reduce average data rate $D_{\mathrm{avg}}^{\mathrm{DL}}$. This indicates the existence of an optimal slot partitioning for maximizing $D_{\mathrm{avg}}^{\mathrm{DL}}$. Similar conclusions can be drawn about the relation between τ_1 and $D_{\mathrm{avg}}^{\mathrm{UL}}$ for a given τ_2. We will discuss more about this optimal slot partitioning in the sequel.

In the next two sections, we will specialize the general results of this section to the downlink and uplink modes, which will provide several useful system design insights.

IV. Downlink Mode

The coverage probability in the downlink mode defined in (6) can be expressed as $P_{\mathrm{cov}}^{\mathrm{DL}} =$

$$\mathbb{E}_{\Phi_b}\Big[\mathbb{P}\Big(\mathrm{SINR}_{\mathrm{DL}} \geq \beta_{\mathrm{DL}}\Big|\Phi_b\Big)\mathbb{P}\Big(E_{\mathrm{H}} \geq \mathcal{E}\big(\tilde{R},\tau_2\big)\Big|\Phi_b\Big)\Big], \tag{19}$$

which is the special case of (8). As discussed in Section II and later explained in Remark 1, $P_{\mathrm{cov}}^{\mathrm{DL}}$ can be derived directly by applying some substitutions, explained in Remark 1, on (16). Similarly, we can derive the energy coverage for downlink mode by applying the same substitutions on (11). We first state this energy coverage result next.

Lemma 4 (Energy Coverage Probability in the Downlink Mode): Probability that the harvested energy during the charging sub-slot is greater than the value $\mathcal{E}(\tilde{R},\tau_2)$ is

$$\begin{aligned} \mathbb{P}\big(E_{\mathrm{H}} \geq \mathcal{E}\big(\tilde{R},\tau_2\big)\big) &= 1 - \pi\lambda_b\mathcal{A}^2\exp\Big(-\pi\lambda_b\mathcal{A}^2\Big) \\ &\quad - \exp\Big(-\pi\lambda_b\mathcal{A}^2\Big) + \int_{\mathcal{A}}^{\infty}\int_{0}^{r_2}\Bigg(\frac{r_2^{\alpha}\exp\big(-r_1^{\alpha}\mathcal{F}_{\mathrm{DL}}(r_1,r_2)\big)}{r_2^{\alpha}-r_1^{\alpha}} \\ &\quad - \frac{r_1^{\alpha}\exp\big(-r_2^{\alpha}\mathcal{F}_{\mathrm{DL}}(r_1,r_2)\big)}{r_2^{\alpha}-r_1^{\alpha}}\Bigg) \\ &\quad \times f_{R_1,R_2}(r_1,r_2)\mathrm{d}r_1\mathrm{d}r_2, \end{aligned} \tag{20}$$

where $f_{R_1,R_2}(r_1,r_2) = (2\pi\lambda_b)^2 r_1 r_2 e^{-\pi\lambda_b r_2^2}$, $\mathcal{F}_{\mathrm{DL}}(r_1,r_2) = C(\tau_1) - \frac{2\pi\lambda_b r_2^{2-\alpha}}{\alpha-2}$, $C(\tau_1) = \frac{\mathcal{E}(\tilde{R},\tau_2)}{\tau_1 T\eta P_{\mathrm{t}}}$, and $\mathcal{A} = \big(\frac{2\pi\lambda_b}{C(\tau_1)(\alpha-2)}\big)^{\frac{1}{\alpha-2}}$.

Proof: See Appendix C. ∎

Remark 3: The effect of the duration of the charging sub-slot $T_{\mathrm{ch}} = \tau_1 T$ appears in the value of $C(\tau_1)$. Consistent with intuition, as this duration increases, the value of $C(\tau_1)$ decreases and the energy coverage probability increases.

We now state the (downlink) coverage result for the downlink mode (defined in (6)).

Theorem 2 (Downlink Coverage Probability in the Downlink Mode): The downlink coverage probability with SINR threshold β_{DL} and minimum required energy $\mathcal{E}(\tilde{R},\tau_2)$ is given by

$$\begin{aligned} P_{\mathrm{cov}}^{\mathrm{DL}} &= \int_0^{\mathcal{A}}\int_0^{r_2} f_{R_1,R_2}(r_1,r_2)\exp\big(-\mathcal{G}(r_1,r_2)\big)\frac{1}{1+\frac{\beta_{\mathrm{DL}}r_1^{\alpha}}{r_2^{\alpha}}}\mathrm{d}r_1\mathrm{d}r_2 \\ &\quad + \int_{\mathcal{A}}^{\infty}\int_0^{r_2} f_{R_1,R_2}(r_1,r_2)\exp\big(-\mathcal{G}(r_1,r_2)\big) \\ &\quad \times \frac{r_2^{\alpha}\exp\big(-r_1^{\alpha}\mathcal{F}_{\mathrm{DL}}(r_1,r_2)\big) - r_1^{\alpha}\exp\big(-r_2^{\alpha}\mathcal{F}_{\mathrm{DL}}(r_1,r_2)\big)}{\big(r_2^{\alpha}-r_1^{\alpha}\big)\Big(1+\frac{\beta_{\mathrm{DL}}r_1^{\alpha}}{r_2^{\alpha}}\Big)}\mathrm{d}r_1\mathrm{d}r_2, \end{aligned} \tag{21}$$

where $\mathcal{G}(r_1,r_2)$ is defined in Lemma 2, $C(\tau_1)$, $\mathcal{A}$, and $\mathcal{F}_{\mathrm{DL}}(r_1,r_2)$ are defined in Lemma 4.

Proof: See Appendix C. ∎

Remark 4: The effect of the duration of the charging sub-slot $T_{\mathrm{ch}} = \tau_1 T$ appears mainly in the value of $\mathcal{A}$ (implicitly in the value of $C(\tau_1)$). It can be observed that as this duration increases, the value of $\mathcal{A}$ increases and $P_{\mathrm{cov}}^{\mathrm{DL}}$ approaches the coverage probability of regularly powered network $P_{\mathrm{cov}}^{\mathrm{DL,RP}} = \mathbb{P}(\mathrm{SINR} \geq \beta_{\mathrm{DL}})$. This is because as T_{ch} increases, it becomes easier to satisfy the energy constraint and the energy coverage probability increases.

Remark 5: Conditioned on Φ_b, the variable $\mathcal{A}$ represents an important system parameter. In (21), it can be interpreted as a threshold on the value of r_2. In particular, as long as the

distance to the second nearest BS (which is also the second dominant RF source on average) is less than this threshold, the energy coverage condition is satisfied and the only condition required for coverage is $\mathrm{SINR_{DL}} \geq \beta_{\mathrm{DL}}$, which is represented by the first term in (21). This useful system insight is a result of using the approximation in (9) that defines the amount of energy harvested in terms of distances r_1 and r_2. This provides useful characterization of the regime in which the performance of this RF-powered IoT network will be similar to the regularly powered network. Similar observations will be provided for the uplink case in the next section.

The general expression for average throughput given in (17) can be specialized for the downlink mode as follows:

$$D_{\mathrm{avg}}^{\mathrm{DL}} = \tau_2 W_D \log(1+\beta_{\mathrm{DL}}) P_{\mathrm{cov}}^{\mathrm{DL}}. \tag{22}$$

Remark 6: Similar to our comments in Remark 2, $R_{\mathrm{avg}}^{\mathrm{DL}}$ is an increasing function of τ_1. On the other hand, the duration $\tau_2 T$ of the downlink sub-slot decreases with increase in τ_1. This indicates the existence of an optimal value of τ_1 that maximizes $D_{\mathrm{avg}}^{\mathrm{DL}}$.

V. Uplink Mode

In this section, we specialize the results of Section III to the uplink mode. Recall that in the uplink mode, each time-slot is partitioning into two sub-slots: charging sub-slot and uplink sub-slot. As discussed in Section II and Remark 1, the uplink coverage probability, defined in (7), can be obtained directly by applying the substitutions explained in Remark 1 on (16). Similar procedure can be used to derive an expression for the energy coverage probability.

While these substitutions are quite similar to the ones that we made in the previous section for the downlink mode, there is a subtle difference in the energy conditions, which is the reason why the final results are slightly different in the two cases. In particular, while the minimum required energy in the downlink mode was fixed ($\mathcal{E}(\tilde{R}, \tau_2)$), it is a function of the nearest BS location in the uplink mode (due to power control). As in the previous section, we first state the energy coverage result for the Uplink mode next.

Lemma 5 (Energy Coverage Probability in the Uplink Mode): Energy coverage probability is

$$\begin{aligned}\mathbb{P}\big(E_{\mathrm{H}} \geq \tau_3 T \rho \|x_1\|^{\epsilon\alpha}\big) &= 1 - \pi\lambda_b \tilde{\mathcal{A}}^2 \exp\Big(-\pi\lambda_b\tilde{\mathcal{A}}^2\Big) \\ &- \exp\Big(-\pi\lambda_b\tilde{\mathcal{A}}^2\Big) + \int_{\tilde{\mathcal{A}}}^{\infty}\int_{0}^{\mathcal{H}(r_2)} f_{R_1,R_2}(r_1,r_2)\mathrm{d}r_1\mathrm{d}r_2 \\ &+ \int_{\tilde{\mathcal{A}}}^{\infty}\int_{\mathcal{H}(r_2)}^{r_2} f_{R_1,R_2}(r_1,r_2)\Bigg(\frac{r_2^{\alpha}\exp\big(-r_1^{\alpha}\mathcal{F}_{\mathrm{UL}}(r_1,r_2)\big)}{r_2^{\alpha}-r_1^{\alpha}} \\ &- \frac{r_1^{\alpha}\exp\big(-r_2^{\alpha}\mathcal{F}_{\mathrm{UL}}(r_1,r_2)\big)}{r_2^{\alpha}-r_1^{\alpha}}\Bigg)\mathrm{d}r_1\mathrm{d}r_2, \end{aligned} \tag{23}$$

where $f_{R_1,R_2}(r_1,r_2) = (2\pi\lambda_b)^2 r_1 r_2 e^{-\pi\lambda_b r_2^2}$, $\mathcal{H}(r_2) = \big(\frac{2\pi\lambda_b}{(\alpha-2)\tilde{C}(\tau_1)}\big)^{\frac{1}{\epsilon\alpha}} r_2^{\frac{2-\alpha}{\epsilon\alpha}}$, $\mathcal{F}_{\mathrm{UL}}(r_1,r_2) = \tilde{C}(\tau_1) r_1^{\epsilon\alpha} - \frac{2\pi\lambda_b r_2^{2-\alpha}}{\alpha-2}$, $\tilde{C}(\tau_1) = \frac{\tau_3\rho}{\tau_1\eta P_t}$, $\tilde{\mathcal{A}} = \big(\frac{2\pi\lambda_b}{\tilde{C}(\tau_1)(\alpha-2)}\big)^{\frac{1}{(\epsilon+1)\alpha-2}}$.

Proof: See Appendix D. ∎

Remark 7: It is easy to see that increasing the density λ_b of the BS PPP Φ_b increases energy coverage probability due to two reasons. First, it reduces the distance r_1 between the typical device and its serving BS, which reduces the transmission power ${r_1}^{\epsilon\alpha}$ of this device, this making it easier to satisfy the energy coverage condition. Second, increasing λ_b also increases the aggregate energy E_{H} harvested by the typical device. This is also evident from (23) where all the terms can be shown to be decreasing functions of λ_b.

We now present the uplink coverage probability (defined in (7)) next. Using this, we will discuss the differences between the regularly powered and energy harvesting networks.

Theorem 3 (Uplink Coverage Probability in the Uplink Mode): The uplink coverage probability $P_{\mathrm{suc}}^{\mathrm{UL}}$ of the IoT device with SINR threshold β_{UL} and uplink transmission power $\rho\|x_1\|^{\epsilon\alpha}$ is $P_{\mathrm{suc}}^{\mathrm{UL}} =$

$$\begin{aligned}&\int_0^{\tilde{\mathcal{A}}}\int_0^{r_2} f_{R_1,R_2}(r_1,r_2) e^{\left(-\frac{\beta_{\mathrm{UL}}\sigma_{\mathrm{UL}}^2}{\rho {r_1}^{(\epsilon-1)\alpha}}\right)} \mathcal{L}_{\tilde{I}_2}\left(\frac{\beta_{\mathrm{UL}}}{{r_1}^{(\epsilon-1)\alpha}}\right)\mathrm{d}r_1\mathrm{d}r_2 \\ &+ \int_{\tilde{\mathcal{A}}}^{\infty}\int_0^{\mathcal{H}(r_2)} f_{R_1,R_2}(r_1,r_2) e^{\left(-\frac{\beta_{\mathrm{UL}}\sigma_{\mathrm{UL}}^2}{\rho {r_1}^{(\epsilon-1)\alpha}}\right)} \mathcal{L}_{\tilde{I}_2}\left(\frac{\beta_{\mathrm{UL}}}{{r_1}^{(\epsilon-1)\alpha}}\right)\mathrm{d}r_1\mathrm{d}r_2 \\ &+ \int_{\tilde{\mathcal{A}}}^{\infty}\int_{\mathcal{H}(r_2)}^{r_2} f_{R_1,R_2}(r_1,r_2) \frac{r_2^{\alpha}\exp\left(-r_1^{\alpha}\mathcal{F}_{\mathrm{UL}}(r_1,r_2) - \frac{\beta_{\mathrm{UL}}\sigma_{\mathrm{UL}}^2}{\rho {r_1}^{(\epsilon-1)\alpha}}\right)}{r_2^{\alpha}-r_1^{\alpha}} \\ &\times \mathcal{L}_{\tilde{I}_2}\left(\frac{\beta_{\mathrm{UL}}}{{r_1}^{(\epsilon-1)\alpha}}\right)\mathrm{d}r_1\mathrm{d}r_2 \\ &- \int_{\tilde{\mathcal{A}}}^{\infty}\int_{\mathcal{H}(r_2)}^{r_2} f_{R_1,R_2}(r_1,r_2) \frac{r_1^{\alpha}\exp\left(-r_2^{\alpha}\mathcal{F}_{\mathrm{UL}}(r_1,r_2) - \frac{\beta_{\mathrm{UL}}\sigma_{\mathrm{UL}}^2}{\rho {r_1}^{(\epsilon-1)\alpha}}\right)}{r_2^{\alpha}-r_1^{\alpha}} \\ &\times \mathcal{L}_{\tilde{I}_2}\left(\frac{\beta_{\mathrm{UL}}}{{r_1}^{(\epsilon-1)\alpha}}\right)\mathrm{d}r_1\mathrm{d}r_2, \end{aligned} \tag{24}$$

where $\mathcal{H}(r_2)$, $\tilde{C}(\tau_1)$, $\mathcal{F}_{\mathrm{UL}}(r_1,r_2)$, and $\tilde{\mathcal{A}}$ are as defined in Lemma 5, and $\mathcal{L}_{\tilde{I}_2}(s)$ is defined in Lemma 3.

Proof: See Appendix C. ∎

By comparing the above result with the uplink coverage probability of the regularly powered network given by (14), we note that the effect of energy harvesting mainly appears in the term $\tilde{\mathcal{A}}$. For instance, if we try to exclude the energy coverage condition ($E_{\mathrm{H}} \geq \tau_3 T\rho\|x_1\|^{\epsilon\alpha}$) by putting $\tau_3 = 0$, we will get $\tilde{C}(\tau_1) = 0$, which will tend $\tilde{\mathcal{A}}$ to ∞. This will eventually make all the terms in (24) tend to zero except the first term which will be equivalent to (14).

Remark 8: Similar to Remark 5, the value of $\tilde{\mathcal{A}}$ here represents a threshold on the distance to the second nearest BS r_2. In particular, as long as $r_2 \leq \tilde{\mathcal{A}}$, the uplink coverage probability of the RF-powered network is exactly the same as that of the regularly powered network. This can be deduced from the first term of (24).

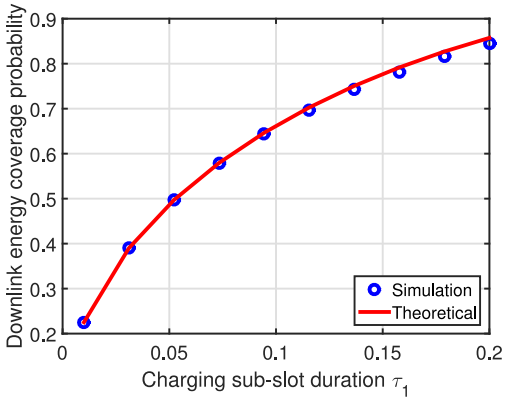

Fig. 3. Energy coverage probability in the downlink mode as a function of τ_1.

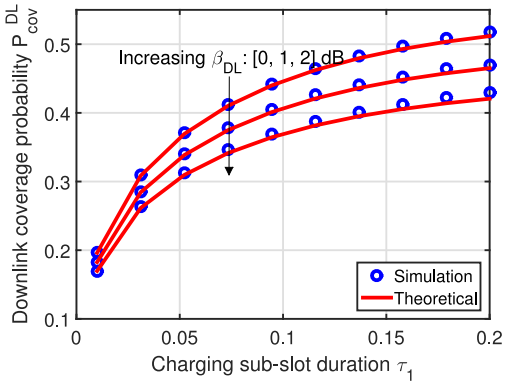

Fig. 4. Downlink coverage probability $P_{\text{cov}}^{\text{DL}}$ in the downlink mode as a function of τ_1.

Similar to (18), the average uplink throughput $D_{\text{avg}}^{\text{UL}} = \tau_3 R_{\text{avg}}^{\text{UL}}$ can be expressed as

$$D_{\text{avg}}^{\text{UL}} = \tau_3 W_U \log(1+\beta_{\text{UL}}) P_{\text{suc}}^{\text{UL}}. \tag{25}$$

Note that, similar to Remark 6, the time-slot division parameter τ_1 has an optimum value that maximizes the throughput $D_{\text{avg}}^{\text{UL}}$. We conclude this section with the following remark.

Remark 9: By comparing the results for downlink and uplink modes (given in Theorems 2 and 3, respectively), with those of the regularly powered network, we conclude that $\mathcal{A} = (\frac{2\pi\lambda_b}{C(\tau_1)(\alpha-2)})^{\frac{1}{\alpha-2}}$ and $\tilde{\mathcal{A}} = (\frac{2\pi\lambda_b}{\tilde{C}(\tau_1)(\alpha-2)})^{\frac{1}{(\epsilon+1)\alpha-2}}$ can be used as tuning parameters for the energy harvesting network. The closer we need the downlink or uplink coverage probability to be to the regularly powered network, the larger the values of $\mathcal{A}$ and $\tilde{\mathcal{A}}$ need to be. These tuning parameters capture in their definitions the effects of all system parameters including P_{t}, λ_b, τ_1, τ_2, τ_3, and η.

VI. Simulation Results and Discussion

Unless specified otherwise, we will consider the following values for the simulation parameters throughout this section: $\mathcal{E}(\tilde{R}, \tau_2) = \tau_2 T(a\tilde{R}^{\epsilon} + b)$ Joules, $a = 10^{-3}$, $b = 5 \times 10^{-4}$, $\lambda_b = 1$, $\alpha = 4$, $\eta = 10^{-3}$, $W_D = 1$ MHz, $\beta_{\text{DL}} = 1$ dB, $P_{\text{t}} = 0$ dB, $\frac{P_t}{\sigma_{\text{DL}}^2} = 20$ dB, $\rho = 1$ dBm, $\frac{\rho}{\sigma_{\text{UL}}^2} = 20$ dB, $\lambda_u = 30\lambda_b$, $\beta_{\text{UL}} = 1$ dB, $\epsilon = 0.8$, and $T = 10^{-2}$ sec.

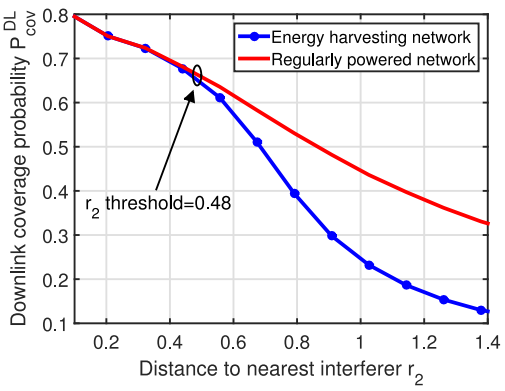

Fig. 5. Downlink coverage probability conditioned on the value of r_2.

A. Downlink Mode

In this subsection, we evaluate the performance of the downlink mode using the performance metrics derived in Section IV. First, in Fig. 3 we plot the energy coverage probability result derived in Lemma 4. As discussed in Remark 3, energy coverage probability is clearly an increasing function of the time division parameter τ_1. The theoretical results are also shown to match perfectly with the simulation results obtained from Monte-Carlo trials, which verifies the accuracy of the dominant BS-based approach used to approximate the energy E_{H} in our analysis. The downlink coverage result derived in Theorem 2 is plotted in Fig. 4. Comparisons with simulation results again verify the accuracy of the dominant BS-based approximation. As discussed in Remark 4, we notice that the coverage probability $P_{\text{cov}}^{\text{DL}}$ starts converging to the coverage probability of regularly powered networks, given by $\mathbb{P}(\text{SINR}_{\text{DL}} \geq \beta_{\text{DL}})$, at high values of τ_1. To glean sharper insights, we recall Remark 5, where we referred to $\mathcal{A}$ as a threshold on the value of distance to the second nearest BS r_2, below which this RF-powered IoT network has the same downlink coverage as the regularly powered network. In Fig. 5, we verify this insight by plotting the coverage probabilities for both RF-powered and regularly powered networks conditioned on r_2 (for $\tau_1 = 0.1$). As predicted in Remark 5, the performance of both the networks is the same when r_2 is below the threshold value, which in this case is $r_2 = \mathcal{A} = 0.48$. Even though this insight was a byproduct of dominant BS-based approximation, we notice that it is remarkably accurate. Right after the threshold value of $r_2 = \mathcal{A} = 0.48$, the two curves start diverging. Finally, we plot our results in (22) for the average throughput in Fig. 6. Comparisons with the simulation results verify the accuracy of our analysis. The results also illustrate the existence of an optimum value for τ_1 that maximizes the average throughput in the downlink mode, as predicted in Remark 6.

B. Uplink Mode

In this section, we focus on the performance analysis of uplink mode. In particular, we will study the effect of τ_1 and λ_b on the performance metrics derived in Section V. In Fig. 7, we plot the energy coverage probability in the uplink mode as a function of λ_b. Consistent with Remark 7, the energy

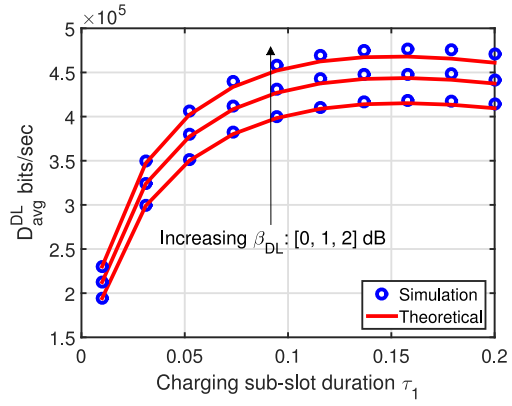

Fig. 6. Downlink average throughput $D_{\text{avg}}^{\text{DL}}$ in the downlink mode as a function of τ_1.

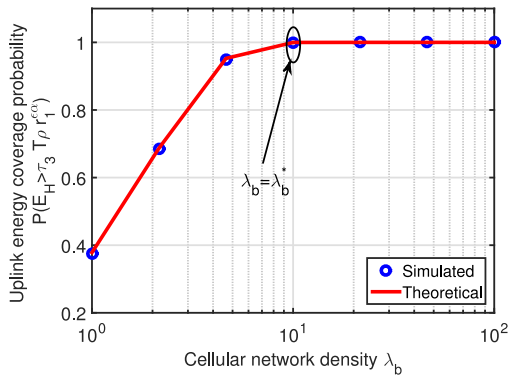

Fig. 7. Uplink energy coverage probability as a function of cellular network density λ_b.

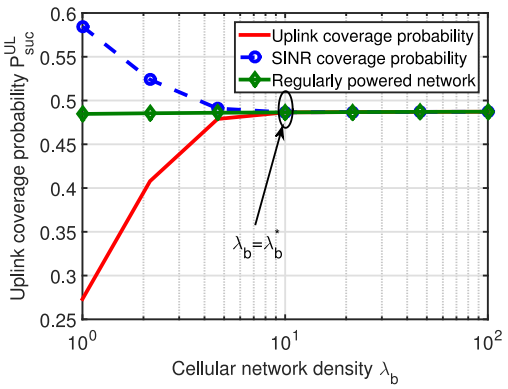

Fig. 8. Uplink coverage probability $P_{\text{suc}}^{\text{UL}}$ in the uplink mode as a function of λ_b.

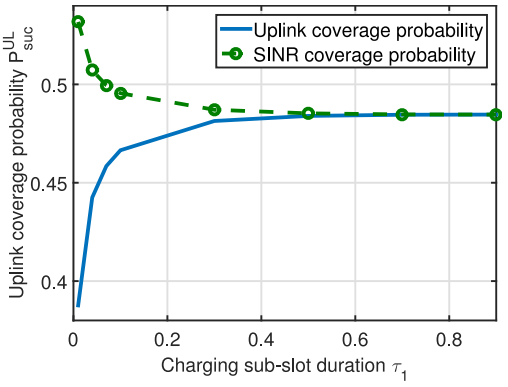

Fig. 9. Uplink coverage probability as a function of uplink time-slot division parameter τ_1.

coverage probability increases with λ_b and saturates to unity when λ_b is above a specific value, which we denote by λ_b^*. Beyond this value of density, the energy coverage condition is satisfied with high probability. Consequently, the uplink coverage probability $P_{\text{suc}}^{\text{UL}}$ is expected to converge to the SINR coverage probability, defined as $\mathbb{P}(\text{SINR}_{\text{UL}} \geq \beta_{\text{UL}})$, at λ_b^*. This is verified in Fig. 8, where starting from $\lambda_b = \lambda_b^*$, the energy coverage condition is satisfied most of the time and the uplink coverage probability reduces to SINR coverage, i.e., $\mathbb{P}(\text{SINR}_{\text{UL}} \geq \beta_{\text{UL}}, E_H \geq \rho r_1^{\epsilon\alpha}) \simeq \mathbb{P}(\text{SINR}_{\text{UL}} \geq \beta_{\text{UL}})$. We also note that the SINR coverage probability in Fig. 8 initially decreases with λ_b until it becomes constant starting from about $\lambda_b = \lambda_b^*$. This is due to the increase in energy coverage probability which leads to increase in the density of active devices, hence increasing the interference value. The value to which they converge starting from $\lambda_b = \lambda_b^*$ is the uplink coverage probability for the case of regularly powered network ($P_{\text{suc}}^{\text{UL,RP}}$ in (14)). Similar trends are observed in Fig. 9, where we note that the uplink coverage and the SINR coverage probabilities converge at about $\tau_1 = 0.5$, which can be interpreted as the minimum value of τ_1 at which the energy coverage condition is satisfied with a high probability. Also, similar to our discussion above on the effect of λ_b, the SINR coverage probability in Fig. 9 initially decreases due to the increase in the energy coverage probability which increases the density of active devices and, consequently, the interference.

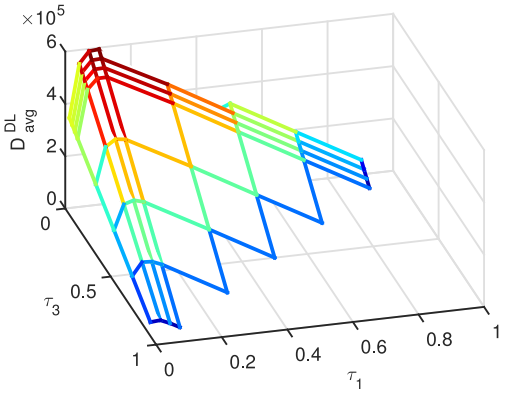

Fig. 10. Downlink average throughput during joint uplink and downlink mode as a function of τ_1 and τ_3.

C. Joint Uplink and Downlink Mode

In Fig. 10 we provide a 3D plot for $D_{\text{avg}}^{\text{DL}}$ as a function of τ_1 and τ_3. Recall that $\tau_2 = 1 - \tau_1 - \tau_3$. We note that for any given value of τ_1, the value of $D_{\text{avg}}^{\text{DL}}$ decreases as τ_3 increases (equivalently τ_2 decreases). As discussed in Remark 2, for any given value of τ_3, there exists optimal τ_1 (and hence optimal τ_2) that maximizes $D_{\text{avg}}^{\text{DL}}$. A similar behavior has already been seen in Fig. 6. Similar observations can be made about the behavior of $D_{\text{avg}}^{\text{UL}}$.

VII. Conclusion

In this paper, we developed an analytical framework to study joint uplink and downlink coverage performance of a cellular-based ambient RF energy harvesting network in which IoT devices are solely powered by the downlink cellular transmissions. Each time-slot is assumed to be partitioned into charging, downlink, and uplink sub-slots. Within each time-slot, the IoT devices (assumed batteryless) first harvest RF energy from cellular transmissions and then use this energy to perform downlink and uplink communication in the subsequent sub-slots. For this setup, we derived the joint probability that the typical device harvests sufficient energy in the charging sub-slot and achieves sufficiently high downlink and uplink SINRs in the following two sub-slots. The main technical contribution is in handling the correlation between these energy and SINR coverage events. Using this result, we also studied system throughput as a function of the time-slot division parameters. Optimal slot partitioning that maximizes this throughput is also discussed. Using these results, we also compared the performance of this RF-powered IoT network with a regularly powered network in which the IoT devices have uninterrupted access to reliable power source, such as a battery. We derived thresholds on several system parameters beyond which the performance of this RF-powered IoT network converges to that of the regularly powered network.

Finally, we defined a *tuning parameter*, which incorporates the effect of all system parameters, and needs to be sufficiently high for the coverage performance of this RF-powered network to converge to that of the regularly powered network.

This work can be extended in multiple directions. From the energy harvesting perspective, the system model can be extended to include rechargeable batteries (with finite capacities) at the devices. This will require explicit consideration of the temporal dimension, as done in [22], where the BSs were assumed to be self-powered with access to batteries with finite capacities. From the modeling perspective, it is important to consider other BS-device configurations, such as the ones in which devices are clustered around the BSs [48].

Appendix A

The value of $\Psi(r_2)$ can be derived as follows:

$$\begin{aligned}\Psi(r_2) &= \mathbb{E}\left[\sum_{x\in\Phi_b\setminus x_1,x_2} g_x\|x\|^{-\alpha}\Big|x_1,x_2\right]\\ &\overset{(a)}{=} \mathbb{E}\left[\sum_{x_i\in\Phi_b\setminus x_1,x_2}\|x_i\|^{-\alpha}\right] \overset{(b)}{=} 2\pi\lambda_b\int_{r_2}^{\infty}\frac{1}{r^{\alpha}}r\mathrm{d}r\\ &= \frac{2\pi\lambda_b}{\alpha-2}({r_2}^{2-\alpha}),\end{aligned} \tag{26}$$

where (a) follows from the assumption that all $\{g_x\}$ are independent and exponentially distributed random variables with mean one, and (b) follows from Campbell's theorem [49] with conversion from Cartesian to polar coordinates and using $r_2 = \|x_2\|$. Using the approximation introduced in (9), the conditional energy coverage probability can be expressed as:

$$\begin{aligned}\mathbb{P}(&E_{\mathrm{H}}\geq E_{\min}|\Phi_b) = \mathbb{P}\Bigg(\tau_1 T\eta P_{\mathrm{t}}\Bigg(g_{x_1}r_1^{-\alpha}+g_{x_2}r_2^{-\alpha}+\frac{2\pi\lambda_b}{\alpha-2}r_2^{2-\alpha}\Bigg)\\ &\geq \mathcal{E}\big(\tilde{R},\tau_2\big)+\tau_3 T\rho r_1^{\epsilon\alpha}\Big)\\ &= \mathbb{P}\Bigg(g_{x_1}r_1^{-\alpha}+g_{x_2}r_2^{-\alpha}\geq C(\tau_1)+\frac{\tau_3\rho r_1^{\epsilon\alpha}}{\tau_1\eta P_{\mathrm{t}}}-\frac{2\pi\lambda_b}{\alpha-2}r_2^{2-\alpha}\Bigg)\\ &= \mathbb{P}\big(g_{x_1}r_1^{-\alpha}+g_{x_2}r_2^{-\alpha}\geq \mathcal{F}(r_1,r_2)\big)\\ &\overset{(c)}{=} \frac{r_2^{\alpha}\exp\big(-r_1^{\alpha}[\mathcal{F}(r_1,r_2)]^{+}\big)-r_1^{\alpha}\exp\big(-r_2^{\alpha}[\mathcal{F}(r_1,r_2)]^{+}\big)}{r_2^{\alpha}-r_1^{\alpha}},\end{aligned} \tag{27}$$

where step (c) is due to hypo-exponential distribution of $g_{x_1}r_1^{-\alpha}+g_{x_2}r_2^{-\alpha}$ (sum of two exponential random variables with rates r_1^{α} and r_2^{α}), $C(\tau_1)=\frac{\mathcal{E}(\tilde{R},\tau_2)}{\tau_1 T\eta P_{\mathrm{t}}}$, and $[x]^{+}=\max\{0,x\}$. This concludes the proof of (10). Noting that $\mathbb{P}(E_{\mathrm{H}}\geq E_{\min}\big|\Phi_b)=1$ when $\mathcal{F}(r_1,r_2)\leq 0$ and integrating over r_1 and r_2 with $f_{R_1,R_2}(r_1,r_2)=(2\pi\lambda_b)^2 r_1 r_2 e^{-\lambda_b\pi {r_2}^2}$ [47], the result in (11) follows.

Appendix B

Using the definition of $\mathrm{SINR}_{\mathrm{DL}}$ in (2) and approximating the interference I_1 by the sum of interference from the nearest interferer and the expectation of the interference from the rest of the interference field, we get

$$\begin{aligned}\mathbb{P}(\mathrm{SINR}_{\mathrm{DL}}\geq\beta_{\mathrm{DL}}|r_1,r_2) &= \mathbb{P}\left(\frac{P_{\mathrm{t}}h_{x_1}\|x_1\|^{-\alpha}}{I_1+\sigma_{\mathrm{DL}}^2}\geq\beta_{\mathrm{DL}}\Big|r_1,r_2\right)\\ &= \mathbb{P}\left(\frac{P_{\mathrm{t}}h_{x_1}r_1^{-\alpha}}{P_{\mathrm{t}}h_{x_2}r_2^{-\alpha}+P_{\mathrm{t}}\Psi(r_2)+\sigma_{\mathrm{DL}}^2}\geq\beta_{\mathrm{DL}}\Big|r_1,r_2\right)\\ &\overset{(d)}{=} \mathbb{P}\left(\frac{P_{\mathrm{t}}h_{x_1}r_1^{-\alpha}}{P_{\mathrm{t}}h_{x_2}r_2^{-\alpha}+P_{\mathrm{t}}\frac{2\pi\lambda_b r_2^{2-\alpha}}{\alpha-2}+\sigma_{\mathrm{DL}}^2}\geq\beta_{\mathrm{DL}}\Big|r_1,r_2\right)\\ &= \mathbb{P}\left(h_{x_1}r_1^{-\alpha}\geq\frac{\beta_{\mathrm{DL}}\sigma_{\mathrm{DL}}^2}{P_{\mathrm{t}}}+\frac{2\pi\lambda_b\beta_{\mathrm{DL}}r_2^{2-\alpha}}{\alpha-2}+\beta_{\mathrm{DL}}h_{x_2}r_2^{-\alpha}\right)\\ &\overset{(e)}{=} \mathbb{E}_{h_{x_2}}\left[\exp\left(-r_1^{\alpha}\left(\frac{\beta_{\mathrm{DL}}\sigma_{\mathrm{DL}}^2}{P_{\mathrm{t}}}+\frac{2\pi\lambda_b\beta_{\mathrm{DL}}r_2^{2-\alpha}}{\alpha-2}+\beta_{\mathrm{DL}}h_{x_2}r_2^{-\alpha}\right)\right)\right]\\ &\overset{(f)}{=} \exp\big(-\mathcal{G}(r_1,r_2)\big)\frac{1}{1+\beta_{\mathrm{DL}}\frac{r_1^{\alpha}}{r_2^{\alpha}}},\end{aligned} \tag{28}$$

where (d) follows from substituting for $\Psi(r_2)$ as derived in (26), and steps (e) and (f) follow from the assumption that $h_x\sim\exp(1)$, and defining $\mathcal{G}(r_1,r_2)=\frac{\beta_{\mathrm{DL}}\sigma_{\mathrm{DL}}^2 r_1^{\alpha}}{P_{\mathrm{t}}}+\frac{2\pi\lambda_b\beta_{\mathrm{DL}}r_2^{2-\alpha}r_1^{\alpha}}{\alpha-2}$.

In the uplink sub-slot, the locations of *active* IoT devices (IoT devices in energy coverage) in a given time-frequency resource can be approximately modeled by the PPP $\tilde{\Phi}_u$ with density $\tilde{\lambda}_u=P_h\times\lambda_b$ where $P_h=\mathbb{P}(E_{\mathrm{H}}\geq E_{\min})$. This will lead to the following expression for $\mathrm{SINR}_{\mathrm{UL}}$:

$$\mathrm{SINR}_{\mathrm{UL}}=\frac{w_o\|x_1\|^{(\epsilon-1)\alpha}}{\sum\limits_{u_i\in\tilde{\Phi}_u\setminus u_o}w_i\Big(R_1^{(i)}\Big)^{\epsilon\alpha}D_i^{-\alpha}+\frac{\sigma_{\mathrm{UL}}^2}{\rho}}. \tag{29}$$

Defining $\tilde{I}_2 = \sum_{u_i \in \tilde{\Phi}_u \setminus u_o} w_i (R_1^{(i)})^{\epsilon\alpha} D_i^{-\alpha}$, we have:

$$\begin{aligned}
\mathbb{P}(\mathrm{SINR}_{\mathrm{UL}} \geq \beta_{\mathrm{UL}} | r_1) &= \mathbb{P}\left(\frac{w_0 {r_1}^{(\epsilon-1)\alpha}}{\tilde{I}_2 + \frac{\sigma_{\mathrm{UL}}^2}{\rho}} \geq \beta_{\mathrm{UL}} | r_1 \right) \\
&= \mathbb{E}_{\tilde{I}_2}\left[\mathbb{P}\left(w_0 \geq \frac{\left(\tilde{I}_2 + \frac{\sigma_{\mathrm{UL}}^2}{\rho}\right)\beta_{\mathrm{UL}}}{{r_1}^{(\epsilon-1)\alpha}} \Big| r_1, \tilde{I}_2 \right) \right] \\
&\overset{(g)}{=} \mathbb{E}_{\tilde{I}_2}\left[\exp\left(-\frac{(\tilde{I}_2 + \frac{\sigma_{\mathrm{UL}}^2}{\rho})\beta_{\mathrm{UL}}}{{r_1}^{(\epsilon-1)\alpha}} \right) \right] \\
&\overset{(h)}{=} e^{\left(-\frac{\beta_{\mathrm{UL}}\sigma_{\mathrm{UL}}^2}{\rho {r_1}^{(\epsilon-1)\alpha}} \right)} \mathcal{L}_{\tilde{I}_2}\left(\frac{\beta_{\mathrm{UL}}}{{r_1}^{(\epsilon-1)\alpha}} \right), \qquad (30)
\end{aligned}$$

where step (g) is due to the assumption that w_0 is exponentially distributed with mean one, and step (h) results from using the Laplace transform of $\tilde{I}_2$, which can be found by replacing λ_b with $\tilde{\lambda}_b = P_h \lambda_b$ in (13), where $P_h = \mathbb{P}(E_{\mathrm{H}} \geq E_{\min})$.

APPENDIX C

We apply the substitutions in Remark 1 for the downlink case to both Lemma 1 and Theorem 1 to get both energy coverage probability and $P_{\mathrm{cov}}^{\mathrm{DL}}$. Applying these substitutions reduces the value of $\mathcal{F}(r_1, r_2)$ to $\mathcal{F}_{\mathrm{DL}}(r_1, r_2) = C(\tau_1) - \frac{2\pi\lambda_b r_2^{2-\alpha}}{\alpha-2}$, where $C(\tau_1)$ is as defined in Lemma 1. Letting $\mathcal{A} = (\frac{2\pi\lambda_b}{(\alpha-2)C(\tau_1)})^{\frac{1}{\alpha-2}}$, we note that the set $\mathcal{N}_{r_2}$ will be empty set for $r_2 \geq \mathcal{A}$ while for $r_2 \leq \mathcal{A}$ the set will be simply $\mathcal{N}_{r_2} = \{r_1 : r_1 \leq r_2\}$. Similarly, the set $\mathcal{P}_{r_2}$ will be empty set for $r_2 \leq \mathcal{A}$ while for $r_2 \geq \mathcal{A}$ the set will reduce to $\mathcal{P}_{r_2} = \{r_1 : r_1 \leq r_2\}$. Applying these integration limits on our result in Lemma 1 leads to the final result in Lemma 4. Similarly, applying these new integration limits to the result in Theorem 1 and noting that the substitutions explained in Remark 1 include $\beta_{\mathrm{UL}} = 0$ (which leads to $\mathcal{L}_{\tilde{I}_2}(0) = 1$ in (16)), the final result in Theorem 2 follows.

APPENDIX D

Similar to the approach in the downlink case, we apply the substitutions in Remark 1 for the uplink case to both Lemma 1 and Theorem 1. Applying these substitutions reduces the value of $\mathcal{F}(r_1, r_2)$ to $\mathcal{F}_{\mathrm{UL}}(r_1, r_2) = \tilde{C}(\tau_1) r_1^{\epsilon\alpha} - \frac{2\pi\lambda_b r_2^{2-\alpha}}{\alpha-2}$, where $\tilde{C}(\tau_1) = \frac{\tau_3 \rho}{\tau_1 \eta P_{\mathrm{t}}}$. Letting $\tilde{\mathcal{A}} = (\frac{2\pi\lambda_b}{\tilde{C}(\tau_1)(\alpha-2)})^{\frac{1}{(\epsilon+1)\alpha-2}}$, we note that the set $\mathcal{N}_{r_2} = \{r_1 : r_1 < (\frac{2\pi\lambda_b}{\tilde{C}(\tau_1)(\alpha-2)})^{\frac{1}{\epsilon\alpha}} r_2^{\frac{2-\alpha}{\epsilon\alpha}}\}$ for $r_2 \geq \tilde{\mathcal{A}}$ while for $r_2 \leq \tilde{\mathcal{A}}$ the set will be simply $\mathcal{N}_{r_2} = \{r_1 : r_1 \leq r_2\}$. Similarly, the set $\mathcal{P}_{r_2}$ will be empty set for $r_2 \leq \tilde{\mathcal{A}}$ while for $r_2 \geq \tilde{\mathcal{A}}$ the set will reduce to $\mathcal{P}_{r_2} = \{r_1 : (\frac{2\pi\lambda_b}{\tilde{C}(\tau_1)(\alpha-2)})^{\frac{1}{\epsilon\alpha}} r_2^{\frac{2-\alpha}{\epsilon\alpha}} \leq r_1 \leq r_2\}$. Applying these integration limits on our result in Lemma 1 leads to the final result in Lemma 5. Similarly, applying these new integration limits to the result in Theorem 1 and noting that the substitutions explained in Remark 1 include $\beta_{\mathrm{DL}} = 0$ (which makes $\mathcal{G}(r_1, r_2) = 0$ in (16)), the final result in Theorem 3 follows.

REFERENCES

[1] M. A. Kishk and H. S. Dhillon, "Downlink performance analysis of cellular-based IoT network with energy harvesting receivers," in *Proc. IEEE GLOBECOM*, Washington, DC, USA, Dec. 2016, pp. 1–6.

[2] A. Whitmore, A. Agarwal, and L. Da Xu, "The Internet of Things: A survey of topics and trends," *Inf. Syst. Front.*, vol. 17, no. 2, pp. 261–274, Apr. 2015.

[3] "Ericsson mobility report: One the pulse of the networked society," Stockholm, Sweden, Ericsson, White Paper, Nov. 2015. [Online]. Available: http://goo.gl/5nSiwt

[4] H. S. Dhillon, H. C. Huang, H. Viswanathan, and R. A. Valenzuela, "Power-efficient system design for cellular-based machine-to-machine communications," *IEEE Trans. Wireless Commun.*, vol. 12, no. 11, pp. 5740–5753, Nov. 2013.

[5] H. S. Dhillon, H. C. Huang, H. Viswanathan, and R. A. Valenzuela, "Fundamentals of throughput maximization with random arrivals for M2M communications," *IEEE Trans. Commun.*, vol. 62, no. 11, pp. 4094–4109, Nov. 2014.

[6] H. S. Dhillon, H. C. Huang, and H. Viswanathan, "Wide-area wireless communication challenges for the Internet of Things," *IEEE Commun. Mag.*, vol. 55, no. 2, pp. 168–174, Feb. 2017.

[7] V. Jelicic, M. Magno, D. Brunelli, V. Bilas, and L. Benini, "Analytic comparison of wake-up receivers for WSNs and benefits over the wake-on radio scheme," in *Proc. 7th ACM Workshop Perform. Monitoring Meas. Heterogeneous Wireless Wired Netw.*, Paphos, Cyprus, Oct. 2012, pp. 99–106.

[8] A. Somov and R. Giaffreda, "Powering IoT devices: Technologies and opportunities," *IEEE IoT Newslett.*, to be published.

[9] K. Huang and X. Zhou, "Cutting the last wires for mobile communications by microwave power transfer," *IEEE Commun. Mag.*, vol. 53, no. 6, pp. 86–93, Jun. 2015.

[10] X. Lu, P. Wang, D. Niyato, D. I. Kim, and Z. Han, "Wireless networks with RF energy harvesting: A contemporary survey," *IEEE Commun. Surveys Tuts.*, vol. 17, no. 2, pp. 757–789, 2nd Quart., 2015.

[11] P. Kamalinejad *et al.*, "Wireless energy harvesting for the Internet of Things," *IEEE Commun. Mag.*, vol. 53, no. 6, pp. 102–108, Jun. 2015.

[12] S. Ulukus *et al.*, "Energy harvesting wireless communications: A review of recent advances," *IEEE J. Sel. Areas Commun.*, vol. 33, no. 3, pp. 360–381, Mar. 2015.

[13] J. G. Andrews, A. K. Gupta, and H. S. Dhillon. (2016). *A Primer on Cellular Network Analysis Using Stochastic Geometry*. [Online]. Available: arxiv.org/abs/1604.03183

[14] H. ElSawy, E. Hossain, and M. Haenggi, "Stochastic geometry for modeling, analysis, and design of multi-tier and cognitive cellular wireless networks: A survey," *IEEE Commun. Surveys Tuts.*, vol. 15, no. 3, pp. 996–1019, 3rd Quart., 2013.

[15] S. Mukherjee, *Analytical Modeling of Heterogeneous Cellular Networks: Geometry, Coverage, and Capacity*. New York, NY, USA: Cambridge Univ. Press, 2014.

[16] H. ElSawy, A. Sultan-Salem, M. S. Alouini, and M. Z. Win, "Modeling and analysis of cellular networks using stochastic geometry: A tutorial," *IEEE Commun. Surveys Tuts.*, vol. 19, no. 1, pp. 167–203, 1st Quart., 2017.

[17] I. Flint, X. Lu, N. Privault, D. Niyato, and P. Wang, "Performance analysis of ambient RF energy harvesting with repulsive point process modeling," *IEEE Trans. Wireless Commun.*, vol. 14, no. 10, pp. 5402–5416, Oct. 2015.

[18] C. Zhong, X. Chen, Z. Zhang, and G. K. Karagiannidis, "Wireless-powered communications: Performance analysis and optimization," *IEEE Trans. Commun.*, vol. 63, no. 12, pp. 5178–5190, Dec. 2015.

[19] K. Huang and V. K. N. Lau, "Enabling wireless power transfer in cellular networks: Architecture, modeling and deployment," *IEEE Trans. Wireless Commun.*, vol. 13, no. 2, pp. 902–912, Feb. 2014.

[20] A. H. Sakr and E. Hossain, "Analysis of K-tier uplink cellular networks with ambient RF energy harvesting," *IEEE J. Sel. Areas Commun.*, vol. 33, no. 10, pp. 2226–2238, Oct. 2015.

[21] Y. L. Che, L. Duan, and R. Zhang, "Spatial throughput maximization of wireless powered communication networks," *IEEE J. Sel. Areas Commun.*, vol. 33, no. 8, pp. 1534–1548, Aug. 2015.

[22] H. S. Dhillon, Y. Li, P. Nuggehalli, Z. Pi, and J. G. Andrews, "Fundamentals of heterogeneous cellular networks with energy harvesting," *IEEE Trans. Wireless Commun.*, vol. 13, no. 5, pp. 2782–2797, May 2014.

[23] K. Ganesan, P. Grover, and J. Rabaey, "The power cost of over-designing codes," in *Proc. IEEE Workshop Signal Process. Syst. (SiPS)*, Beirut, Lebanon, Oct. 2011, pp. 128–133.

[24] C. G. Blake and F. R. Kschischang, "Energy consumption of VLSI decoders," *IEEE Trans. Inf. Theory*, vol. 61, no. 6, pp. 3185–3198, Jun. 2015.
[25] P. Grover, "Bounds on the tradeoff between decoding complexity and rate for sparse-graph codes," in *Proc. IEEE Inf. Theory Workshop (ITW)*, Tahoe City, CA, USA, Sep. 2007, pp. 196–201.
[26] I. Krikidis, "Simultaneous information and energy transfer in large-scale networks with/without relaying," *IEEE Trans. Commun.*, vol. 62, no. 3, pp. 900–912, Mar. 2014.
[27] X. Zhou, R. Zhang, and C. K. Ho, "Wireless information and power transfer: Architecture design and rate-energy tradeoff," *IEEE Trans. Commun.*, vol. 61, no. 11, pp. 4754–4767, Nov. 2013.
[28] S. Zhou, T. Chen, W. Chen, and Z. Niu, "Outage minimization for a fading wireless link with energy harvesting transmitter and receiver," *IEEE J. Sel. Areas Commun.*, vol. 33, no. 3, pp. 496–511, Mar. 2015.
[29] M. Di Renzo and W. Lu, "System-level analysis and optimization of cellular networks with simultaneous wireless information and power transfer: Stochastic geometry modeling," *IEEE Trans. Veh. Technol.*, vol. 66, no. 3, pp. 2251–2275, Mar. 2017.
[30] T. A. Khan, A. Alkhateeb, and R. W. Heath, "Millimeter wave energy harvesting," *IEEE Trans. Wireless Commun.*, vol. 15, no. 9, pp. 6048–6062, Sep. 2016.
[31] M. M. Shaikh and M. C. Aguayo-Torres, "Joint uplink/downlink coverage and spectral efficiency in heterogeneous cellular network," *Wireless Pers. Commun.*, vol. 95, no. 2, pp. 233–244, Jul. 2017.
[32] K. Yang, P. Wang, X. Hong, and X. Zhang, "Joint downlink and uplink network performance analysis with CRE in heterogeneous wireless network," in *Proc. IEEE PIMRC*, Hong Kong, Aug./Sep. 2015, pp. 1659–1663.
[33] S. Singh, X. Zhang, and J. G. Andrews, "Joint rate and SINR coverage analysis for decoupled uplink-downlink biased cell associations in HetNets," *IEEE Trans. Wireless Commun.*, vol. 14, no. 10, pp. 5360–5373, Oct. 2015.
[34] O. Ozel and S. Ulukus, "AWGN channel under time-varying amplitude constraints with causal information at the transmitter," in *Proc. IEEE Asilomar*, Pacific Grove, CA, USA, Nov. 2011, pp. 373–377.
[35] E. MolavianJazi and A. Yener, "Low-latency communications over zero-battery energy harvesting channels," in *Proc. IEEE GLOBECOM*, San Diego, CA, USA, Dec. 2015, pp. 1–6.
[36] J. G. Andrews, F. Baccelli, and R. K. Ganti, "A tractable approach to coverage and rate in cellular networks," *IEEE Trans. Commun.*, vol. 59, no. 11, pp. 3122–3134, Nov. 2011.
[37] Y. P. E. Wang *et al.*, "A primer on 3GPP narrowband Internet of Things," *IEEE Commun. Mag.*, vol. 55, no. 3, pp. 117–123, Mar. 2017.
[38] X. Zhang and J. G. Andrews, "Downlink cellular network analysis with multi-slope path loss models," *IEEE Trans. Commun.*, vol. 63, no. 5, pp. 1881–1894, May 2015.
[39] A. Arafa and S. Ulukus, "Optimal policies for wireless networks with energy harvesting transmitters and receivers: Effects of decoding costs," *IEEE J. Sel. Areas Commun.*, vol. 33, no. 12, pp. 2611–2625, Dec. 2015.
[40] M. Haenggi, "User point processes in cellular networks," *IEEE Wireless Commun. Lett.*, vol. 6, no. 2, pp. 258–261, Apr. 2017.
[41] S. Weber, J. G. Andrews, and N. Jindal, "The effect of fading, channel inversion, and threshold scheduling on ad hoc networks," *IEEE Trans. Inf. Theory*, vol. 53, no. 11, pp. 4127–4149, Nov. 2007.
[42] P. Madhusudhanan, J. G. Restrepo, Y. Liu, T. X. Brown, and K. R. Baker, "Downlink performance analysis for a generalized shotgun cellular system," *IEEE Trans. Wireless Commun.*, vol. 13, no. 12, pp. 6684–6696, Dec. 2014.
[43] J. Schloemann, H. S. Dhillon, and R. M. Buehrer, "Toward a tractable analysis of localization fundamentals in cellular networks," *IEEE Trans. Wireless Commun.*, vol. 15, no. 3, pp. 1768–1782, Mar. 2016.
[44] T. Bhandari, H. S. Dhillon, and R. M. Buehrer, "The impact of proximate base station measurements on localizability in cellular systems," in *Proc. IEEE SPAWC*, Edinburgh, U.K., Jul. 2016, pp. 1–5.
[45] V. V. C. Ravi and H. S. Dhillon, "Downlink coverage probability in a finite network of unmanned aerial vehicle (UAV) base stations," in *Proc. IEEE SPAWC*, Edinburgh, U.K., Jul. 2016, pp. 1–5.
[46] V. V. C. Ravi and H. S. Dhillon, "Downlink coverage analysis for a finite 3-D wireless network of unmanned aerial vehicles," *IEEE Trans. Commun.*, vol. 65, no. 10, pp. 4543–4558, Oct. 2017.
[47] D. Moltchanov, "Distance distributions in random networks," *Ad Hoc Netw.*, vol. 10, no. 6, pp. 1146–1166, Aug. 2012.
[48] C. Saha, M. Afshang, and H. S. Dhillon, "Enriched *K*-tier HetNet model to enable the analysis of user-centric small cell deployments," *IEEE Trans. Wireless Commun.*, vol. 16, no. 3, pp. 1593–1608, Mar. 2017.
[49] M. Haenggi, *Stochastic Geometry for Wireless Networks*. Cambridge, U.K.: Cambridge Univ. Press, 2012.

Mustafa A. Kishk (S'16) received the B.Sc. and M.Sc. degrees in electronics and electrical communications engineering from Cairo University, Egypt, in 2013 and 2015, respectively. He is currently pursuing the Ph.D. degree with the Bradley Department of Electrical and Computer Engineering, Virginia Tech. His research interests include stochastic geometry, energy harvesting wireless networks, and physical layer security.

Harpreet S. Dhillon (S'11–M'13) received the B.Tech. degree in Electronics and Communication Engineering from IIT Guwahati, India, in 2008; the M.S. degree in Electrical Engineering from Virginia Tech, Blacksburg, VA, USA, in 2010; and the Ph.D. degree in Electrical Engineering from the University of Texas at Austin, TX, USA, in 2013. In academic year 2013-14, he was a Viterbi Postdoctoral Fellow at the University of Southern California, Los Angeles, CA, USA. He joined Virginia Tech in August 2014, where he is currently an Assistant Professor of Electrical and Computer Engineering. He has held internships at Alcatel-Lucent Bell Labs in Crawford Hill, NJ, USA; Samsung Research America in Richardson, TX, USA; Qualcomm Inc. in San Diego, CA, USA; and Cercom, Politecnico di Torino in Italy. His research interests include communication theory, stochastic geometry, geolocation, and wireless *ad hoc* and heterogeneous cellular networks.

Dr. Dhillon is a Clarivate Analytics Highly Cited Researcher and has coauthored five best paper award recipients including the 2016 IEEE Communications Society (ComSoc) Heinrich Hertz Award, the 2015 IEEE ComSoc Young Author Best Paper Award, the 2014 IEEE ComSoc Leonard G. Abraham Prize, and two conference best paper awards at IEEE ICC 2013 and European Wireless 2014. His other academic honors include the 2017 Outstanding New Assistant Professor Award from the Virginia Tech College of Engineering, the 2013 UT Austin Wireless Networking and Communications Group (WNCG) leadership award, the UT Austin Microelectronics and Computer Development (MCD) Fellowship, and the 2008 Agilent Engineering and Technology Award. He currently serves as an Editor for the IEEE TRANSACTIONS ON WIRELESS COMMUNICATIONS, the IEEE TRANSACTIONS ON GREEN COMMUNICATIONS AND NETWORKING, and the IEEE WIRELESS COMMUNICATIONS LETTERS.